Department for Biomedical Sciences at the University of Veterinary Medicine Vienna

Institute of Laboratory Animal Science
(Head: Univ.-Prof. Dr. Thomas Rülicke)

Tomographic optical imaging to study the biodistribution of macromolecular drug carriers in a syngeneic mouse tumor model

Diploma Thesis

University of Veterinary Medicine Vienna

Submitted by
Folie Moritz

Vienna, September 2021

Supervisor: Univ.-Prof. Dr. Thomas Rülicke; Institute of Laboratory Animal Science, University of Veterinary Medicine, Vienna

External Supervisor: Univ.-Prof. Dipl. Ing. Dr. Manfred Ogris; Division of Clinical Pharmacy and Diagnostics, University of Vienna

External Co- Supervisor: Dr. Haider Sami; Division of Clinical Pharmacy and Diagnostics, University of Vienna

Reviewer: Univ.-Prof. Dr. Maik Dahlhoff; Institute for in-vivo and in-vitro models, University of Veterinary Medicine, Vienna

Table of Contents

1 Introduction

An essential part of the drug discovery and development process are biodistribution studies in preclinical animal models. (Peterson et al. 2016) Those are very important to forecast therapeutic safety and efficacy. (Arms et al. 2020) The biodistribution of macromolecules can be studied by a number of possibilities. (Geyer et al. 2017a) *In vivo* imaging, ex vivo imaging and histological examination are used, to investigate the biodistribution of samples labelled with a fluorescent marker in organs and tissues. (Zhang 2016)

In vivo optical imaging is commonly regarded as a qualitative measure of biodistribution. (Arms et al. 2020) With two-dimensional (2D) imaging settings it is often not possible to quantify and exactly localize measured signals. (Geyer et al. 2017a) Three-dimensional (3D) images, in contrast to 2D images, enable volumetric localization and a precise quantification. (Lauber et al. 2017) In addition, the combination of fluorescence imaging tomography with micro CT allows an accurate anatomical allocation of the measured signals. (Geyer et al. 2017a)

1.1 *In vivo* Imaging

The principle of 3Rs (Replacement, Reduction, Refinement) by Russel and Burch is a highly relevant and a valuable tool to improve the quality of the collected data and the life of the animals used in experiments. (De Angelis et al. 2019) The principle builds the ethical basis of the Directive 2010/63/EU on the protection of animals used in scientific research. (De Angelis et al. 2019) Imaging of cancer has become an essential and valuable instrument in preclinical and clinical settings. (Condeelis und Weissleder 2010) Through using different imaging techniques, the number of animals in a scientific investigation can be reduced significantly, which is in full agreement with the ethical efforts of the 3Rs. (Lauber et al. 2017)

In preclinical research and modern drug development imaging devices have become more popular and have turned to essential tools. (Lauber et al. 2017) The number and usage of various imaging methods has explosively grown over the last three decades. (Condeelis und Weissleder 2010) Imaging systems can be classified in different ways. For example in the energy the imaging systems use to acquire the visual information (sound waves, photons, positrons, X-rays), in the spatial resolution achieved (macro-, microscopic) or in the type of information received (anatomic, physiological, molecular/cellular). (Condeelis und Weissleder

2010) Each imaging technique has its specific strength and its limitations. To enhance visualization and data reconstruction hybrid imaging platforms are being developed, which enables for example imaging where anatomical and molecular information can be combined. (Condeelis und Weissleder 2010)

Commonly used in clinical and preclinical use are macroscopic imaging systems to achieve physiological and anatomical information, like computed tomography (CT), ultrasound (US) and magnetic resonance imaging (MRI). Bioluminescence imaging (BLI) and fluorescence imaging (FLI) are molecular imaging systems especially in preclinical and experimental use. (Condeelis und Weissleder 2010) To monitor the (reporter) gene expression and to track cell growth as well as tumor dissemination patterns in small animals bioluminescence and fluorescence is commonly used. (Xu und Rice 2009)
In vivo imaging technologies offer the opportunity to study biological processes of a living organism on a molecular level in real time over a certain time frame. *In vivo* imaging modalities gives the possibility to make non-invasive images with precise and high quantitative anatomical and functional information to monitor the progression of diseases and the response to therapy in animal models. (Lauber et al. 2017)

1.2 Computer tomography (CT)

The CT-prototype was invented by Hounsfield in 1969, it has improved considerably over the last 25 years and is in preclinical and clinical use for more than a half century. (Key und Leary 2014, Hindelang et al. 2015)
CT-scanner are using X-ray beams to produce images using the difference of photon attenuation between materials. (Key und Leary 2014) A computer calculates the attenuation for single tissue elements (voxel) and reconstruct three dimensional images. (Lauber et al. 2017) The wavelength from X-rays, a form of electromagnetic radiation, are between 10 to 0.1 nanometers. They are generated in a vacuum tube by the collision of high energy electron with a tungsten metal. X-rays can be produced by two different atomic processes from these collisions. The quick slowing down of the high energy electrons when they interact with the repulsive electron field of the target metal, generates X-rays, known as *bremsstrahlung*. Apart from that X-rays are also generated from the interaction of the atomic orbitals of the tungsten metal with high energy free electrons. (PerkinElmer Health Sciences 2012) The majority of the electrons instead of X-rays are producing heat. (Bashore 2001) Therefore the X-ray tube has

to resist and deduce enough heat to generate a sufficiently high X-ray radiation for imaging. (Zink 1997) If X-rays encounter matter atoms scatter in new directions, this scattered radiation and the primary beam need to be completely blocked from outside the imaging chamber, due to the hazardous potential to living organisms. (PerkinElmer Health Sciences 2012)

Clinical imaging devices are not able to image small animals like mice or rats precisely, due to the low spatial resolution, the poor tissue contrast and the low sensitivity as well as the size of the animals. The micro-CT for small-animal imaging in preclinical research was developed, with specific enhancements and modification to the instrumentation to manage these limitation, to optimize the signal to noise ratio (SNR) and to achieve the highest spatial resolution possible. (Lauber et al. 2017)

Computed tomography is the ideal imaging device for tissues with significant differences in the density, but the distinction of soft tissue is difficult due to the similar densities. To increase the visibility of specific organs or tissues contrast agents can be used. (Lauber et al. 2017)
Iodine based contrast agents are commonly used because they offer not only an excellent soft tissue contrast, but are also easy to handle and cost effective. (Rawson et al. 2020) The limitation of iodinated small molecules is that the imaging time is shortened due to the rapid renal clearance. To increase the circulation time iodinated organic molecules were combined with nanoparticles, like for example liposomes and lipoproteins. (Key und Leary 2014)

1.3 Optical Imaging

Optical imaging (OI) is used to get molecular and functional information. Optical imaging methods are easy to use, affordable, fast and have a high sensitivity and good temporal and spatial resolution. (Xu und Rice 2009, Arms et al. 2020) The usage of optical imaging methods has increased exponentially during the last 5-10 years. (Kunjachan et al. 2013) In optical imaging either molecules which have to be excited externally to emit photons (fluorescence) or molecules who act as a light source per se (bioluminescence) are used. (Lauber et al. 2017) The light emitted is captured by a ultrasensitive CCD camera. (Tseng et al. 2017) Optical imaging techniques, like fluorescence and bioluminescence imaging have established as very important methods in biomedical research and are commonly used in a variety of research fields, especially in oncological research. (Müller et al. 2013, Etrych et al. 2016, Lauber et al. 2017)

1.3.1 Bioluminescence Imaging (BLI)

The phenomenon of the enzymatic production of light (bioluminescence) appears in many non-mammalian species, like in *Photinus pyralis* (North American Firefly), *Renilla reniformis* (Sea pansy) (Sato et al. 2004) and *Gaussia princeps* (a marine copepod). (Yao et al. 2018) Luciferases act as enzymes and catalyze the oxidation of a substrate releasing photons in the visible range on the spectrum as a by-product. (Lauber et al. 2017, Yao et al. 2018) The chemical reaction between firefly luciferase and its substrate luciferin produces light terms of bioluminescence which can permeate tissue through different depths and skin and allows due to the high selectivity, sensitivity and resolution, the observation of physiological or pathological processes *in vivo*. (Li et al. 2021)

Bioluminescence imaging (BLI) is based on the detection of light emission from tissues and cells and enables longitudinal monitoring of disease processes in the same animal, for example to observe tumor cell growth and dissemination patterns, infections and treatment responses. (Sato et al. 2004) It allows the detection of <100 luciferase marked cells and is therefore one of the most sensitive techniques to detect tumor cells and to observe the tumor progression. (Geyer et al. 2017b)

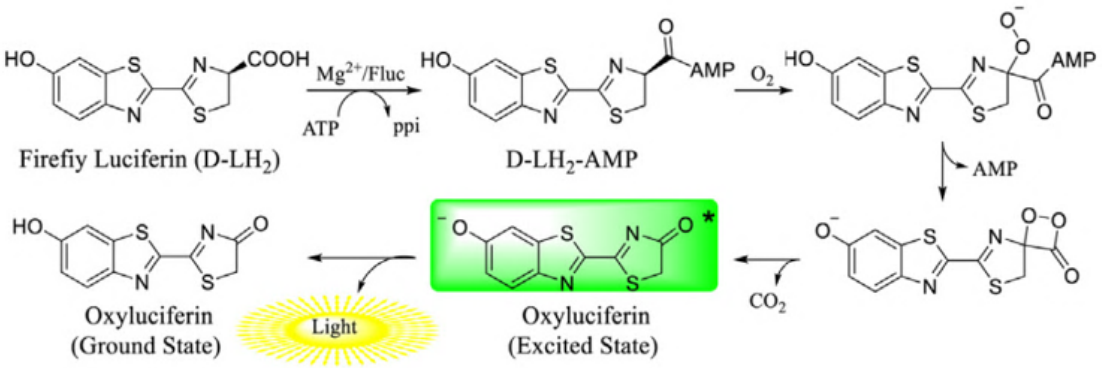

Figure 1 Mechanism of firefly bioluminescence. *First the reaction to emit light requires the substrate D-Luciferin, Adenosine triphosphate (ATP) and Mg^{2+} and the catalyzing enzyme firefly luciferase to produce D-LH_2-AMP. This intermediate state is then oxidized and decarboxylated to produce the unstable excited oxyluciferin which emits light relaxing to the ground state. (Li et al. 2021)*

The biochemical process needs molecular oxygen, luciferin, luciferase and cofactors such as ATP and Mg^{2+}. (Badr und Tannous 2011) The enzyme luciferase reacts with the substrate D-Luciferin creating oxyluciferin which releases photons of light, while converting into the non-reactive state. (Greer und Szalay 2002, Lauber et al. 2017) The emitted light is detected by ultra-sensitive cameras called charge-coupled device. (Sato et al. 2004)

The substrate D-Luciferin is injected intraperitoneally, subcutaneously or intravenously. (Sato et al. 2004, Badr und Tannous 2011, Lauber et al. 2017) Depending on the route of administration the optimal time for imaging changes. The imaging should start instantly after the intravenous application. If the substrate is injected intraperitoneally the imaging session should start 10-30 minutes afterwards due to the slower distribution of the substrate in the organism. Choosing the intraperitoneal route, the signal peaks around 10 minutes after application and stays on a nearly constant level for 30 min. (Badr und Tannous 2011) The subcutaneous application of D-Luciferin is also possible with a maximum signal peak after 20-40 minutes. (Geyer et al. 2017b)

The light emitted from the living subject is captured by a CCD camera. (Tseng et al. 2017) To maintain the required temperature of -90°C a thermoelectric water chiller is used. (PerkinElmer Health Sciences 2012) The reduction of the temperature is necessary to minimize thermal noises. (Sato et al. 2004)

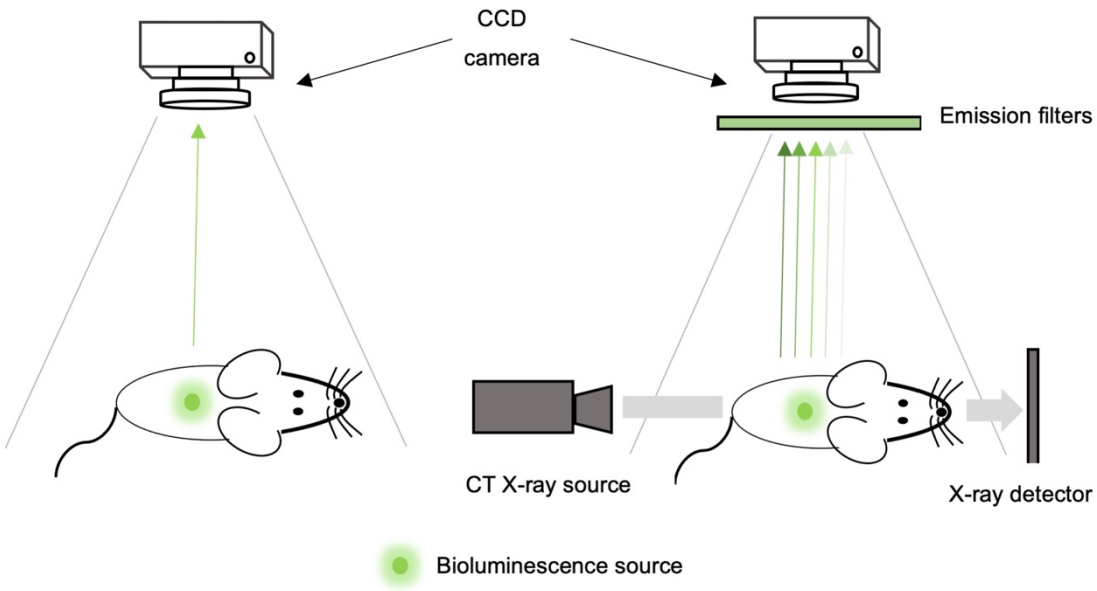

Figure 2 Scheme of 2D bioluminescence Imaging (left) and 3D bioluminescence imaging: DLIT (right). *Figure adapted from (Tseng et al. 2017)*

For the 2D bioluminescence settings no emission filters are required (open filter mode) for imaging. (Tseng et al. 2017) As there is no background noise in the animal tissue, this method exhibits an excellent signal-to-noise-ratio. (Manni et al. 2019) A photographic image is useful

to locate the measured emission signal in the animal. (Sato et al. 2004). The emission filters are used in three-dimensional imaging for a series of 2D bioluminescence surface radiance images at different wavelengths. In addition, the micro-CT is necessary to receive an anatomical context to the bioluminescence signal. A software is reconstructing the 3D tomography using the CT data and an algorithm, based on the variating light emission signals measured in the 2D images to locate the bioluminescence signal in the animal. (Tseng et al. 2017)

To track cells and tissues using BLI a genetic modification is required to enable them the expression of luciferases. A promoter and the expression cassette with the luciferase gene have to be transfected into the cells of interest. If the transfection is successful, the cells are able to produce the enzyme luciferase. The engineered cells can be injected into a mouse and after inducing the light production by adding a substrate it is possible to monitor non-invasively the distribution and location of the cells and the intensity of the light signal. (Sato et al. 2004)

1.3.1.1 CT26F-Luc tumor model

A leading cause of cancer mortality and one of the most commonly diagnosed cancer is the colorectal carcinoma (CRC). (Groza et al. 2018) Nearly one million people are developing CRC every year. (Weitz et al. 2005) At late stages, due to the metastatic lesions a systemic chemotherapy is often not efficient. (Groza et al. 2018) For the development of new therapeutics and to improve the understanding of cancers preclinical tumor models are used. (Castle et al. 2014)

The CT26 colorectal carcinoma cell line is very often used in drug development studies. The CT26 model is a syngeneic *in vivo* test system in BALB/c mice. (Castle et al. 2014) The intraperitoneal (i.p) injection of CT26 cells in BALB/c mice cause tumors distributed within the peritoneal cavity with the tendency to colonize the pancreatic area. (Groza et al. 2018) The study of tumor growth, metastasis and therapeutic responses *in vivo* is possible due to the possibility of tracking modified tumor cells using BLI. (Sato et al. 2004)

1.3.2 Fluorescence Imaging (FLI)

The fastest growing imaging technique is eventually the fluorescence area. For the *in vivo* use technologies for micro- and macroscopy are being adapted. (Condeelis und Weissleder 2010) In preclinical research *in vivo* FLI has become the most commonly utilized tool. (Leblond et al. 2010) Compared to bioluminescence, in fluorescence imaging an additional light source is needed to excite the fluorophores. (Tseng et al. 2017)

The different fluorescent probes available are fluorescent dyes, metallic nanoparticles, quantum dots and fluorescent proteins. The fluorophores commonly used are Alexa Fluor, cyanine dyes, fluorescein and coumarin. (Etrych et al. 2016) Each fluorophore has specific excitation and emission wavelength. (Tseng et al. 2017) The right excitation wavelength for the fluorescent agent is achieved by using filters in front of a light source. (Zelmer und Ward 2013) The excited fluorophore then emits photons at a certain increased wavelength. (Lauber et al. 2017) The light emitted from the fluorophores is detected by a CCD camera equipped with specific emission filters adjusted to the emission wavelength of the fluorescent marker used. (Zelmer und Ward 2013)

Labelling with fluorescent dyes allows to track the spatio-temporal distribution using fluorescence imaging, but tissue autofluorescence and other effects, like background noises from food ingredients, complicates the imaging *in vivo*. (Geyer et al. 2017a) The tissue autofluorescence is produced by the excitation light and occurs in the most tissues (Xu und Rice 2009, Arms et al. 2020) To reduce the fluorescence background noises at least 2 weeks before imaging the mice have to be fed with a low fluorescence diet, due to ingredients regular mouse food has, like chlorophyll which has fluorescent properties. (PerkinElmer Health Sciences 2017) In addition, also hemoglobin and other compounds have a high absorption in the visible range of light. This is why it is necessary to use fluorescence dyes emitting light in the near infrared (NIR) and far-red spectrum. (Geyer et al. 2017a) The optical window used for *in vivo* imaging ranges from 650 to 950 nm. (Moreno et al. 2020)

Two different types of fluorescence imaging are usually used *in vivo*: the reflectance (epi-illumination) and the tomographic (transillumination) mode. (Frangioni 2003) Using the epi-illumination mode, the excitation light is distributed on the surface of the subject. (Frangioni 2003, Xu und Rice 2009) The light source and the detection device are on the same side of

the object. (Leblond et al. 2010) This mode is perfectly suited to measure the emitted fluorescence light from superficial located fluorophores. The problem is that signals from deeper located agents can be disguised by the strong light absorption and autofluorescence. (Xu und Rice 2009) An established method for the enhancement of the contrast and sensitivity is the spectral unmixing, where the fluorescent signal of interest is separated from the tissue background noise. (Xu und Rice 2009)

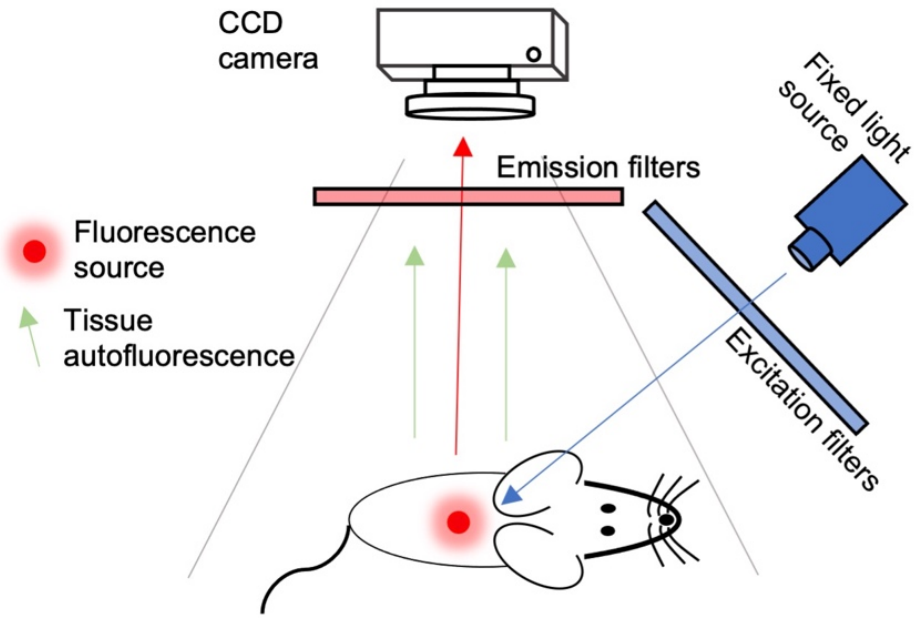

Figure 3 Set-up of the 2D fluorescence imaging: epi-illumination. *Figure adapted from (Tseng et al. 2017)*

The second *in vivo* fluorescence imaging configuration is the transillumination mode. The transillumination mode is detecting the emitted light that passed from one to the other side of the subject, usually a whole animal. (Leblond et al. 2010) The light source is placed on the opposite side of the detection device at the bottom of the stage under the object platform. (Tseng et al. 2017) The transillumination mode is more sensitive for fluorophores located deeper in the tissue. (Xu und Rice 2009, Leblond et al. 2010, Tseng et al. 2017). The autofluorescence is in comparison to the epi-illumination mode reduced due to the fact that the autofluorescence is generated first of all from the bottom surface of the object, where the light source is located. (Xu und Rice 2009) The autofluorescence produced by the reflection from the surface does not get to the CCD which enhances the signal-to-noise ratio. (Zelmer und Ward 2013)

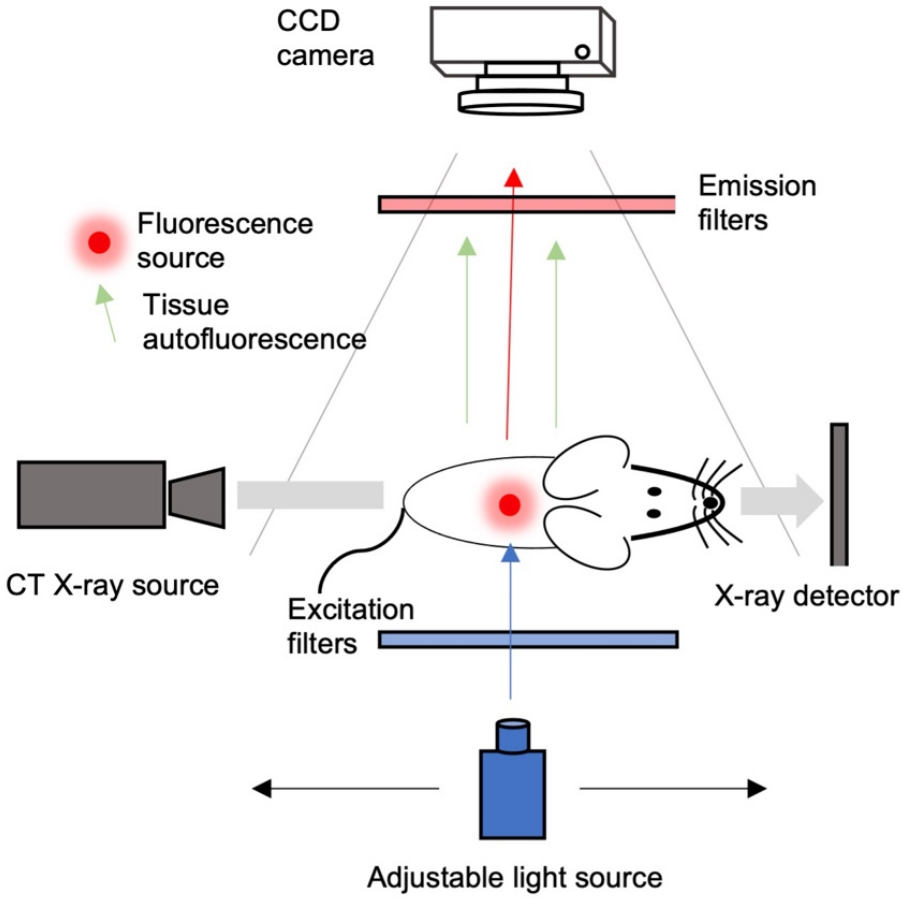

Figure 4 Set-up of the fluorescence imaging tomography (FLIT): transillumination mode. *Figure adapted from (Tseng et al. 2017)*

For quantitative fluorescence imaging tomography the transillumination mode is used. (Condeelis und Weissleder 2010, Geyer et al. 2017a) This method is often combined with CT to improve the image visualization (Condeelis und Weissleder 2010) A combination of FLIT/CT allows an accurate allocation to anatomical structures and a quantification of the signal. (Geyer et al. 2017a)

1.3.3 Multimodal Imaging (Imaging device)

In this thesis, the *in vivo* imaging instrument IVIS Spectrum CT (Perkin Elmer Health Sciences, Waltham, Massachusetts, USA) was used for anatomical and molecular imaging. The setup includes a micro-CT, a fluorescence light source, emission/excitation filters, a high-sensitive CCD (charged coupled device) camera, for the detection of the photons using optical imaging,

and a heated platform for the animals, to grant the maintenance of the physiological body temperature during imaging under anesthesia. (PerkinElmer 2012) The device has the ability of two dimensional bioluminescent and fluorescent imaging (epi- and transillumination) and in addition in combination with the integrated CT it enables a 3D tomography with anatomical context. (Tseng et al. 2017)

The ultra-fast micro-CT, using an x-ray tube source and a CMOS X-ray detector, is generating three-dimensional images of the anatomical structures of mice. During the imaging process the animal stage is moving from the bottom up and rotating. (PerkinElmer Health Sciences 2012)

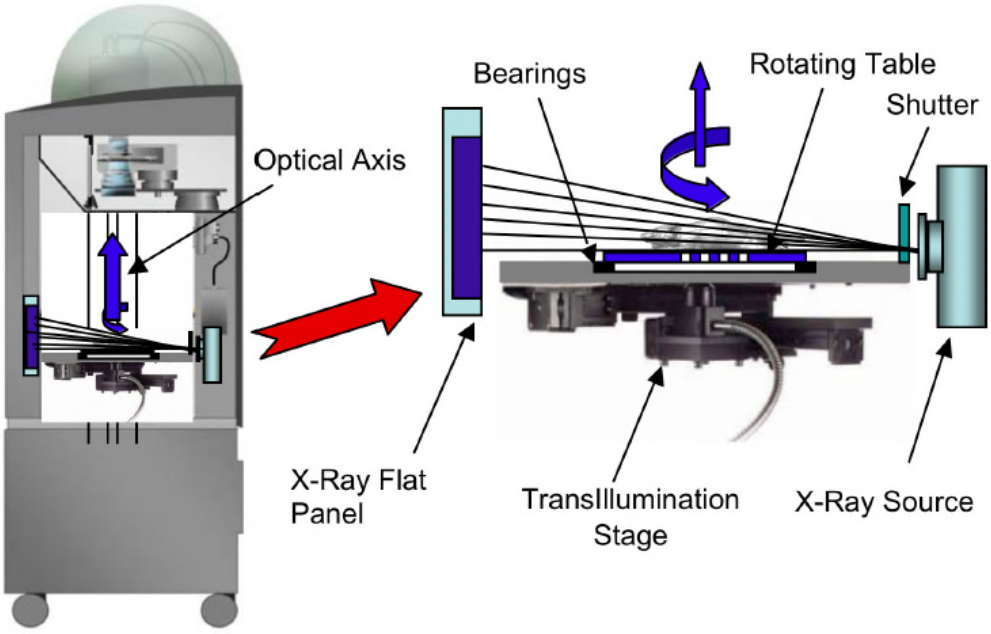

Figure 5 Micro-CT device. *(PerkinElmer Health Sciences 2012)*

To produce the excitation light for fluorescence imaging a 150-Watt tungsten quartz halogen lamp with a dichroic reflector is installed. The output of the lamp is filtered with different fluorescence excitation filters, which can be selected using the Living Image software. The imaging device can use the reflectance or the transillumination mode for fluorescence imaging. Through an optical switch the filtered light is directed to one of the user-selectable holes in the aperture plate at the bottom of the stage, if transillumination is selected, or if epi-illumination is preselected is evenly distributed from the top of the imaging chamber to achieve an even platform illumination. (PerkinElmer Health Sciences 2012)

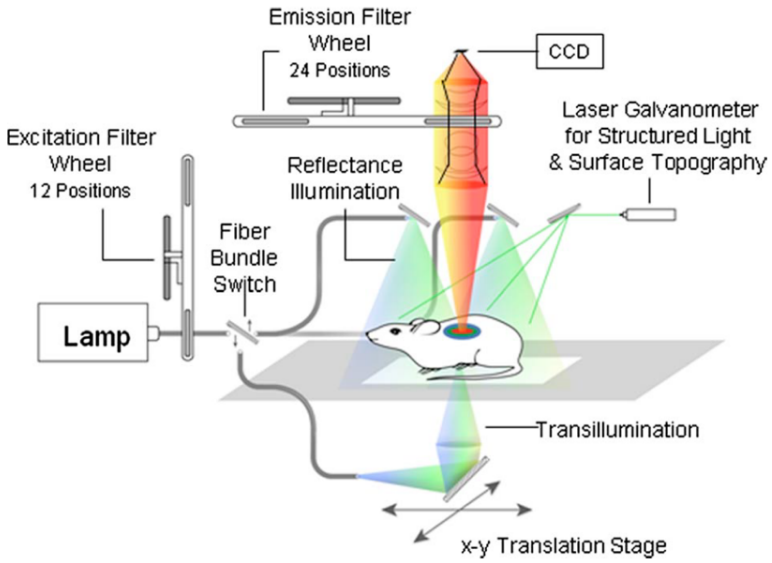

Figure 6 Illustration of the fluorescence imaging system of the IVIS Spectrum imaging device. *(Xu und Rice 2009)*

1.4 Drug delivery systems (DDS)

Drug delivery systems are very useful to reduce toxic and unwanted side effects of strong drugs against cancer or other diseases. Various DDS were developed, like liposomal systems and polymeric micro- and nanoparticles. (Paukner et al. 2006) A very promising drug delivery system to transport drugs for cancer treatment are bacterial ghosts. In comparison with other DDS they have a higher targeting specificity for certain tissues. (Youssof et al. 2019) The most drug delivery systems have to be labeled with a fluorophore for fluorescence imaging. (Etrych et al. 2016) After the application of a labeled drug delivery system (DDS), it is possible to observe the biodistribution by imaging at certain time points. (Etrych et al. 2016)

1.4.1 Bacterial Ghosts as Drug Carriers

Envelopes that are produced by lysis from Gram-negative bacteria are called bacterial ghosts (BGs). (Langemann et al. 2010) In the common method the BGs are produced by the controlled expression of a gene from the enterobakteriophage Phi X 174 (ΦX174), in particular the lysis gene E. (Youssof et al. 2019, Zhang et al. 2019) The role of gene E in the lysis was discovered in 1966. The expression of gene E outside the host range of the bacteriophage, converts Gram-

negative bacteria into ghosts and kills Gram-positive bacteria without lysis. (Langemann et al. 2010) When the lysis gene E is expressed, a transmembrane tunnel is formed. Through that tunnel the cytoplasmic material is removed by osmosis, creating an empty shell. (Ganeshpurkar et al. 2014) Due to the absence of the cytoplasmic material of the bacteria, the bacterial ghosts have no infectious potential. (Kudela et al. 2010) They are not toxic and are well tolerated. (Groza et al. 2018) The BGs still have bio-adhesive surface characteristics which allows the interaction with the hosts immune response cells, like macrophages, monocytes and dendritic cells. Due to that BGs can trigger a cellular and humoral immune response. (Ganeshpurkar et al. 2014) For immunization purposes many bacterial ghosts have been used such as *Pasteurella multocida, Pasteurella haemolytica, Helicobacter pylori* and *Salmonella enteritidis*. (Ganeshpurkar et al. 2014)

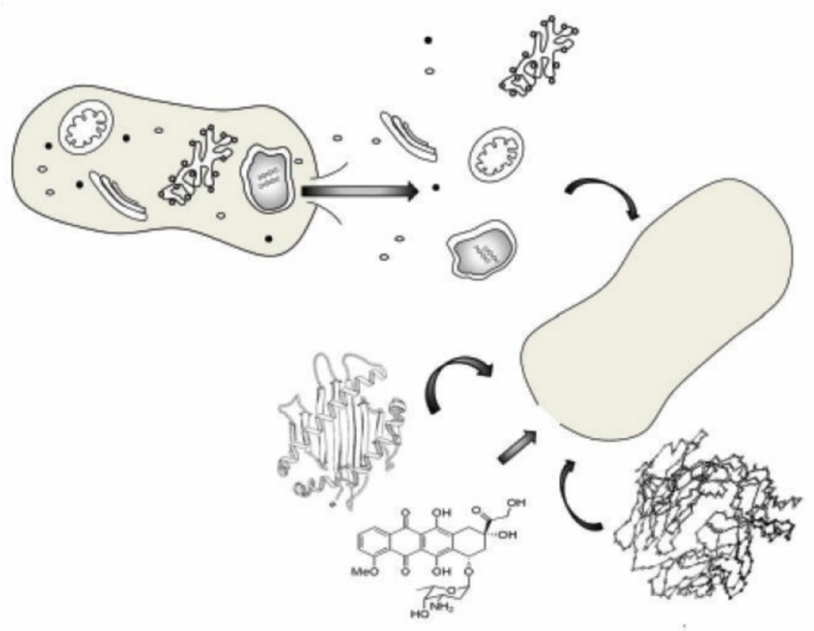

Figure 7 Illustration of the BG production. *After the removal of the cytoplasmic content, the BGs can be loaded with drugs, nucleic acids, antigens, proteins and peptides and used as a delivery system. (Ganeshpurkar et al. 2014)*

In addition, BGs are able to deliver proteins, pharmaceuticals, antigens and nucleic acids. (Ganeshpurkar et al. 2014) They can carry single components or a combination of them. (Kudela et al. 2010) BGs can be loaded with hydrophobic or water-soluble drugs. (Paukner et al. 2006) BGs as a drug delivery system are perfectly suited to transport cytotoxic substances for tumor therapy. (Kudela et al. 2010, Ganeshpurkar et al. 2014)

2 Aim of the Thesis

Optical imaging allows studying the biodistribution of macromolecular drug carriers when labelled with near infrared fluorescent dyes. While two-dimensional, epifluorescence imaging allows a non-quantitative estimation of the biodistribution, tomographic imaging by fluorescence imaging tomography (FLIT) gives an inside view of both quantitative estimation and precice organ allocation of the signals. We hypothetise that FLIT will allow to correlate tumor localization and the accumulation of labelled macromolecular carriers.

In the experiment bioluminescence imaging was used to detect the tumors and observe their progression at several time points in a syngeneic mouse model, by using the CT26 colorectal carcinoma cell line transfected with firefly luciferase. Fluorescence imaging was used to study the biodistribution of a macromolecular drug carrier, in this case bacterial ghosts labelled with AlexaFluor750.

3 Materials and methods

3.1 Animals

The mice of the strain BALB/cJRj (purchased from Janvier Labs, Route du Genest, 53940 Le Genest-Saint-Isle, France), used for the experiment, were bred in-house, weaned and ear-punched four weeks after birth. All mice were housed under specific pathogen free conditions in individually ventilated cages with a 12/12-hour light/dark cycle an air humidity of 60 RH and a constant temperature of 22 degrees Celsius. The air handling unit Smart Flow *(Smart Flow, Tecniplast Deutschland GmbH, Hohenspeißenberg, Germany)* was used to grant the ventilation and to monitor specific parameters (humidity/temperature).

Autoclaved water and food were given ad libitum. Due to the planned FLI imaging they were set from maintenance food *(standard rodent diet, ssniff Spezialdiäten GmBH, Soest, Germany)* on a Low fluorescent diet *(E-15710-047, EF AIN 76A, ssniff Spezialdiäten GmBH, Soest, Germany)* for at least 2 weeks before imaging, to minimize background noises on the images based on plant components in the maintenance food. (PerkinElmer Health Sciences 2017)

Bedding material *(Premium scientific bedding, SAFE, j. Raettenmaier & Söhne GmbH + CoKG, Rosenberg, Germany),* red houses (*Mouse house, Tecniplast Deutschland GmbH, Hohenspeißenberg, Germany)* and nesting material (autoclaved kitchen roll *(Kitchen-roll Easy, FRIPA Papierfabrik Albert Friedrich KG, Miltenberg, Germany)* were the standard equipment for each cage *(Individually ventilated cages, Blue Line 1285L, Tecniplast Deutschland GmbH, Hohenspeißenberg, Germany)*. Those items were added as enrichment into the cage to improve their living conditions and to ensure a natural behavior, like burrowing, exploring, gnawing and nest building, which are essential to the well-being of the animals. Everything that got in contact with the mice was autoclaved before or disinfected with 70% Ethanol, if autoclaving was not possible. The mice were handled under a laminar flow hood *(CS5 EVO GP changing station, Tecniplast Deutschland GmbH, Hohenspeißenberg, Germany)*. In the daily animal check water, food and welfare were monitored. Small injuries from fighting were treated with polyvinyl pyrrolidone Iodine *(Braunol®, 7,5 % solution, B. Braun Melsungen AG, Melsungen, Germany).*

With the start of the experiment also the body weight was measured on every imaging day. The purchased Animal Facility Software PyRat *(Scionics Computer Innovation GmbH, Dresden, Germany)* was used to document all relevant information about the animals (e.g. body weight, treatment, breeding, experiment, birth etc.).

All animals used were shaved with an Aesculap clipper *(cordless clipper Isis Aescluap ®, GT421, Albert Kerbl GmbH, Buchbach, Germany)*, i.e. prone and supine on the lateral parts of the thorax and abdomen on Day -1 and if required immediately before imaging to enhance the imaging quality. Hair removal increases the light capture by the high-sensitive CCD camera. Depilation is advantageous for the image quality, in 3D BLI depilation improves the signal output and the reconstruction accuracy and in 3D FLI hair has an effect on the quality and on the quantitative results. (Tseng et al. 2017) Six female mice between 63 and 85 weeks old were used for this project.

Table 1 Animals of the BG project. *The animals MCT-351, MCT-399 and MCT-415 are the control animals (C1-3). The other animals were treated with BGs (T1-3) on Day 13 (more detailed in Fig.8).*

Mouse ID	Strain	Gender	Age at experimental start
MCT- 351 (C1)	BALB/cJRj	female	85 weeks
MCT- 399 (C2)	BALB/cJRj	female	72 weeks
MCT- 411 (T1)	BALB/cJRj	female	70 weeks
MCT- 414 (T2)	BALB/cJRj	female	63 weeks
MCT- 415 (C3)	BALB/cJRj	female	63 weeks
MCT- 416 (T3)	BALB/cJRj	female	63 weeks

The Experiment (Animal experimentation permission number: 66.006/0027-WF/V/3b/2014) was structured as shown in the following graphic.

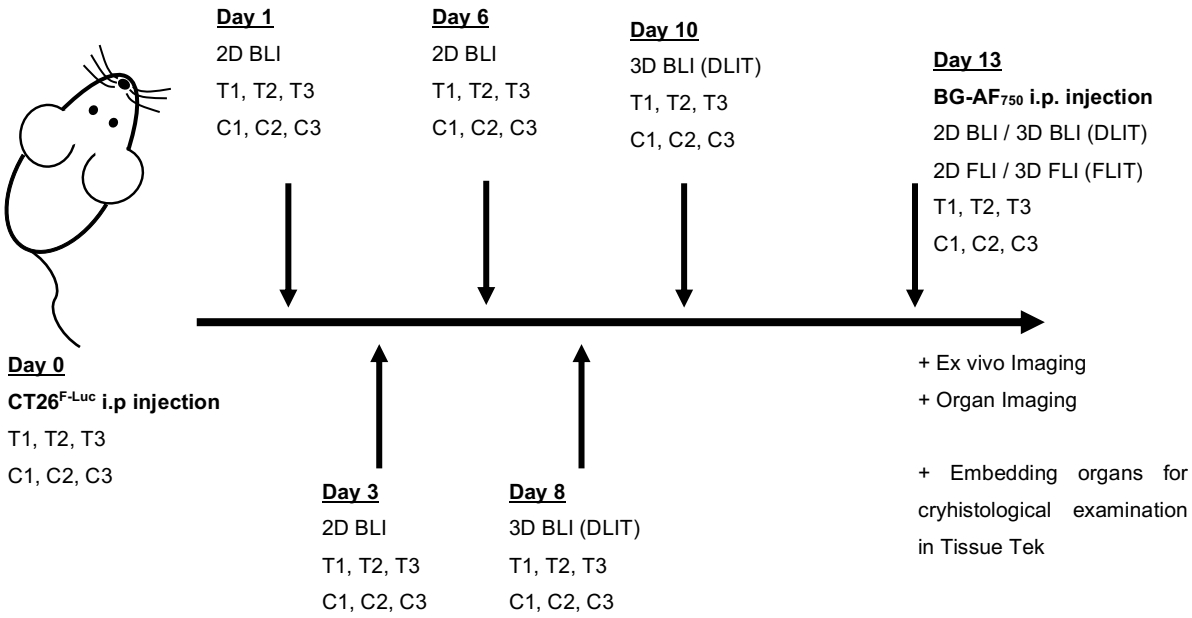

Figure 8 Timeline for the BG project. *8 female BALB/cJRj mice were injected intraperitoneally with CT26$^{F\text{-}Luc}$ on Day 0. The tumor progression was controlled using bioluminescence imaging. On Day 13 the mice from the treated group have received the BGs intraperitoneally and were imaged 2h after the application. Afterwards the animals were sacrificed, the organs were imaged in situ and ex vivo (2D FLI) and were embedded in Tissue Tek for cryohistological examination.*

On Day 13, two mice (control + treated) were always injected and imaged together following the timeline in Figure 9a and 9b.

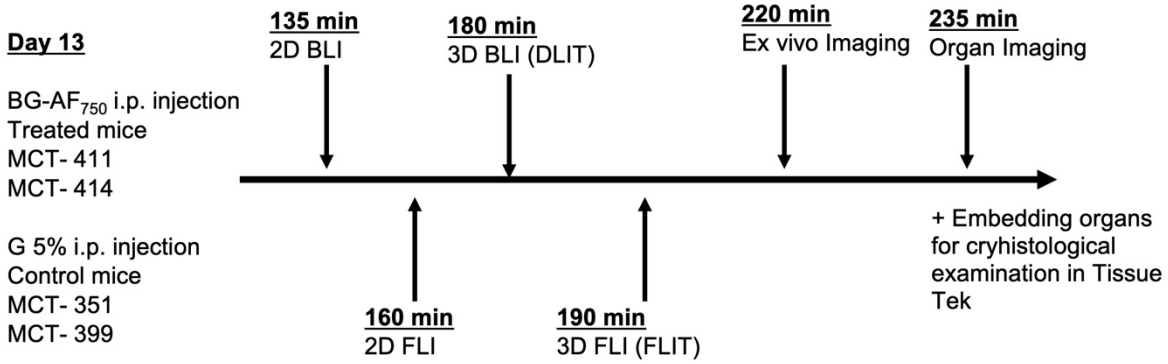

Figure 9a

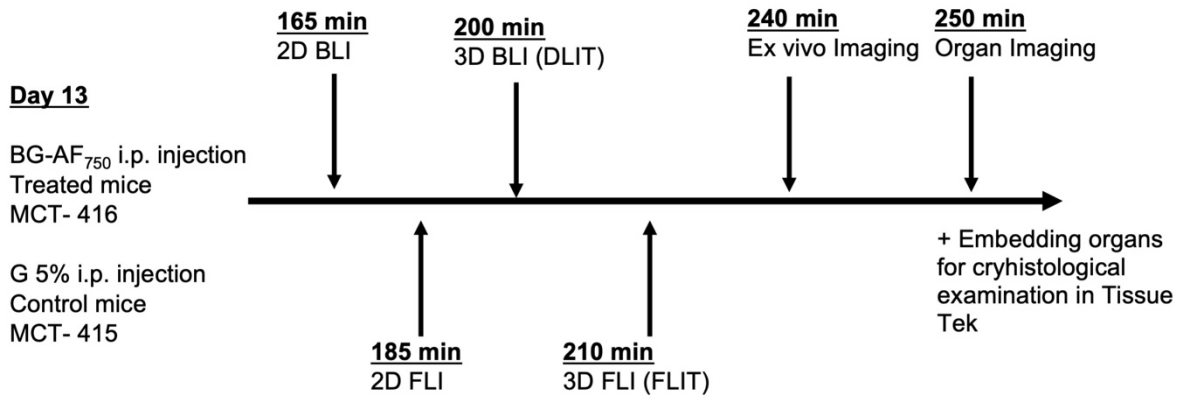

Figure 9b

Figure 9a / 9b: Timeline of Day 13. *The control animals after the application of G 5% intraperitoneally where imaged using 2D BLI and 2D FLI with the treated animals. In addition, the treated animals were separately imaged with FLIT and DLIT. Afterwards the animals of the control and of the treated group were sacrificed and the organs were imaged in situ and ex vivo. For the ex vivo imaging the organs were placed on a black plate. In each session the organs of two mice were imaged simultaneously with FLI (the organs of the BGs treated mouse together with the organs of the control animal). Afterwards the organs were embedded in Tissue Tek for cryohistological examination.*

3.2 Administration procedure

3.2.1 Administration of $CT26^{F\text{-}Luc}$ tumor cells

Intraperitoneal injection of a luciferase marked colon carcinoma tumor cell line (1×10^5 $CT26^{F\text{-}Luc}$ (200 µl)) after resuspending and homogenous swinging the cells on the day of inoculation (Day 0) under a laminar flow hood (Microbiological Safety Cabinet, BIOSAFE 5-130, Ehret GmbH Life Science Solutions, Freiburg i. Br., Germany) into the right lower abdomen. Oxaliplatin, a cytostatic drug which is commonly used as a treatment in advanced colorectal cancer, was initially planned as treatment to prevent the mice from a too high tumor load, but due to the slow tumor growth the Oxaliplatin was not needed.

3.2.2 Administration of bacterial ghosts

The bacterial ghosts were applied intraperitoneally into the right lower abdomen after imaging a black 96 well plate with labelled BGs, unlabeled BGs and a Buffer (5 % Glucose) to control if they were labelled correctly with the fluorescent AF750. To check it 2D FLI Imaging under

following setting was used after vortexing the vials and transferring 100 µl of every sample into a black 96 well plate. Imaging Subject: Well Plate; Spectral Unmixing: Excitation (640nm / 675 nm), Emission (680nm, 700 nm, 729 nm, 740 nm, 760nm / 720nm, 740 nm, 760nm, 780nm, 800nm); Stage C; Segments: Auto; auto delay (max. 300s); Exposure: Auto, Binning: 8; F_{Stop}:2

Table 2 Schematic illustration of the 96-well plate. *The 96-well plate was imaged before the BGs were injected intraperitoneally in the mice, to control the labelling with AF750.*

	1	2	3	4	5	6	7	8	9	10	11	12
A												
B			AF750 labeled BG(100 µl)		AF750 labeled BG(100 µl)		AF750 labeled BG(100 µl)					
C												
D			Unlabeled BG(100 µl)		Unlabeled BG(100 µl)		Unlabeled BG(100 µl)					
E												
F			Buffer G5% (100 µl)		Buffer G5% (100 µl)		Buffer G5% (100 µl)					
G												
H												

From a prepared tube with 1500 µl, 300 µl were taken out and 250 µl BG-AF750 were injected under the laminar flow hood into the right lower abdomen. The control group was injected with 250 µl Glucose 5% (G 5%) also prepared in a tube with 1500 µl where 300 µl were taken out and 250 µl were injected under the laminar flow hood into the right lower abdomen. The imaging session of the mice started two hours after the injection.

24 hours prior imaging 15 ml Gastrografin (contrast agent) *(Gastrografin, 37g Iod/100 ml, Bayer AG, Leverkusen, Germany)* was applied ad 200 ml water bottles. Gastrografin (370mg/ml) treatment was planned to increase at the imaging session the next day. A short period after treatment the mice behavior changed (e.g. running in circles and got diarrhea), due to that the application of Gastrografin was stopped.

3.3 Anesthesia and Imaging procedure

For the *in vivo* imaging process, the mice needed to be anesthetized. For the anesthesia a non-rebreathing system was used. Isoflurane was used as anesthetic agent and oxygen as carrier gas. Every animal was placed in a small induction chamber *(Anesthesia induction*

chamber, PS-0351-SIK, Rothacher-Medical GmbH, Heinenried, Switzerland) with an initial isoflurane *(Isofluran CP® 1ml/ml, cp-pharma, Burgdorf, Germany)* concentration of 5% and an oxygen flow rate of 5L/min for the induction, after reaching a suitable depth of anesthesia the Vaporizer (*Isoflurane Vaporizer, Serial-Nr. 081848, Rothacher & Partner, Berne, Switzerland)* was turned back to reduce the Isoflurane concentration to 2- 2,5% with an oxygen flow rate of 2L/min. If necessary, the concentration was adjusted during the anesthesia. Eyes were protected with an eye ointment *(VitA-POS®, 5g eye ointment with Vitamin A, Ursapharm, Saarbrücken, Germany)*. The imaging (BLI, DLIT, FLI, FLIT) was done by using the IVIS Spectrum µCT *in vivo* imaging system (Perkin Elmer ®). The anesthetized mice were placed during the imaging session on a black non-reflecting heating plate integrated in the IVIS Spectrum imaging device and during the wake-up phase on an extern heating plate *(Heating plate, 1328C-01, Physitemp Instruments, LLC, NJ 07013, United States)* to ensure a physiological body temperature.

3.3.1 Bioluminescence imaging (BLI)

Bioluminescence imaging was used to control the tumor progression and location after injecting all mice with a luciferase marked colon carcinoma tumor cell line which stably express Luciferase ($CT26^{F\text{-}Luc}$) intraperitoneally on Day 0. (Groza et al. 2018) Therefore, the mice were imaged pairwise on day 1, 3 and 6 in 2D BLI. The mice were taken separately out of their cages into the small induction chamber under the laminar flow hood. Then they were anesthetized as described above. The mice received the eye ointment, body mass was measured with a scale *(CS Series (CS200), 72212663, Ohaus Corporation, NJ 07054, United States)* and Luciferin *(D-Luciferin, Potassium salt Vivo Trace™, Intrace Medical SA, Lausanne, Switzerland)* was injected subcutaneously into the neck area before fixing them with a non-reflecting black tape on all four extremities and tail to the heating platform in the IVIS Spectrum CT. The anesthesia was maintained during this procedure and the imaging session with an isoflurane concentration of 2% with a flow of 2 L oxygen per minute. The 2D session was consisted of ten images with a delay of three minutes. Detailed information about the imaging settings in the Tab. 3.

Table 3 *Settings 2D BLI in IVIS Spectrum Imaging Device*

Settings 2D Bioluminescence Imaging	
Emission	Open filter
Animal position	Supine
Field of View (FOV) / Stage	C
Segments	10
Delay	3 min
Subject height	1,5 cm

On Day 8 and 10 mice were imaged in 3D due to the stronger signal to get a more detailed visualization about the tumor size and main location. For DLIT every mouse was imaged individually. The mice were prepared the same way as for 2D BLI. In addition, the animals received 300 µl Iopamidol *(Iopamidol, Unilux® 300 mg Jod/ml, Sanochemia Pharmazeutika AG, Neufeld an der Leitha, Austria)* (a mixture of 180µl glucose *(Glucose, 50 mg/ml, B. Braun Melsungen AG, Melsungen, Germany)* and 120µl Iopamidol) intraperitoneally before starting the imaging session. Iopamidol was used as an iodine-based contrast agent to improve the delimitation of the organs. The 3D imaging session was consisted of five images with an auto delay of maximal 300 sec. and a CT scan at medium resolution. Detailed information about the imaging settings in Tab. 4.

Table 4 *Settings DLIT IVIS Spectrum Imaging Device*

Settings 3D Bioluminescence Imaging (DLIT)	
Filter	560 nm, 580 nm, 600 nm, 620 nm, 640 nm
Animal position	Supine
Field of View (FOV) / Stage	B
Segments	5

Delay	Auto (max. 300 sec)
CT	Medium resolution
Subject height	1,5 cm

D-Luciferin *(D-Luciferin, Potassium salt Vivo Trace™, Intrace Medical SA, Lausanne, Switzerland)* was applied subcutaneously with a single use insulin syringe (*1 ml single-use insuline syringe, Omnican® 100, B. Braun Melsungen AG, Melsungen, Germany)* at the neck area 10 minutes before BLI imaging, to ensure an optimal detection of the CT26$^{F\text{-}Luc}$ cells. The Luciferin was dissolved in DPBS *(Dulbecco's Phosphate Buffered Saline, Sigma-Aldrich, St. Louis, Missouri, United States)* to a concentration at 30 mg per ml The amount of Luciferin was individually calculated regarding the body weight of the mice (dose of 120 mg/kg).

3.3.2 Fluorescence imaging (FLI)

Fluorescence imaging was used to verify the biodistribution of the injected bacterial ghosts. The mice were imaged pairwise on day 13 immediately after the 2D BLI Imaging session to have a direct comparison between the treated mouse (right side) and the control animal (left side). Mice were prepared the same way as for the bioluminescence images except that no D-Luciferin injection was needed. The 2D session was consisted of automatically determined number of images (in total 9). Detailed information about the imaging settings in Tab. 5.

Table 5 *Setting 2D FLI IVIS Spectrum Imaging Device*

Settings 2D Fluorescence Imaging	
Exposure	Auto
Animal position	Supine
Field of View (FOV)	C
Segments	Auto (9)
Delay	Auto

Binning	8
F_{Stop}	2
Spectral Unmixing (SU)	
Excitation	640nm / 675 nm
Emission	680nm, 700 nm, 729 nm, 740 nm, 760nm / 720nm, 740 nm, 760nm, 780nm, 800nm

On Day 13 the treated mice were imaged in 3D due to obtain a better overview on the BGs biodistribution. For the FLIT 3D imaging every mouse was imaged individually directly after the 3D bioluminescence imaging session. Mice were prepared the same way as for the bioluminescence images except that no Luciferin injection was needed. Iopamidol was used as a contrast agent to improve the delimitation of the organs and was injected before the 3D fluorescence imaging was started intraperitoneally.

The 3D imaging session consisted of 13 transillumination points with auto delay and an CT scan at medium resolution. Detailed information about the imaging settings in Tab. 6.

Table 6 *Settings FLIT IVIS Spectrum Imaging Device*

Settings 3D Fluorescence Imaging (FLIT)	
Animal position	Supine
Field of View (FOV)	B
Delay	Auto
Subject height	1.5 cm
CT	Medium resolution
Transillumination points	13

3.3.3 Euthanasia and ex vivo organ imaging

D-Luciferin was applied subcutaneously with a single use insulin syringe at the neck area 10 minutes prior euthanasia to achieve an optimal enzymatic kinetic during imaging. For euthanasia mice were put under deep isoflurane anesthesia in the small induction chamber with an initial isoflurane concentration of 4% and an oxygen flow at 4L/min. Then the concentration was turned back to 2 % isoflurane for ten minutes before the euthanasia was performed by cervical dislocation. For the dissection mice were immobilized on a Styrofoam using four cannulas, one for each extremity. Forceps (anatomical or chirurgical) and a dissection scissor were needed. First of all, the animals were skinned, and the abdomen was opened. A 2D bioluminescence ex vivo overview image was taken to locate the tumors. Afterwards the organs were removed and arranged on a black plate for the organ imaging session. In each session the organs of two mice were imaged simultaneously, on the right side the organs of the with BGs treated mouse were placed and on the left side the organs from the control animal. The organs were imaged 2D BLI and 2D FLI under following settings.

Table 7 *Settings organ imaging (BLI).*

Settings 2D Bioluminescence Organ Imaging	
Emission	Open filter
Excitation	Block
Field of View (FOV)	C
Segments	1
Subject height	0,5 cm

Table 8 *Settings organ imaging (FLI).*

Settings 2D Fluorescence Organ Imaging	
Focus	Manual Focus
F_{Stop}	8
Field of View (FOV)	C
Segments	1
Subject height	0,3 or 0,4 cm

Depending on the signal strength of each organ the organs with the highest signal was removed from the black plate before reimaging the remaining organs.
After removing the organs from the black plate, they were embedded with cryomedium TissueTek *(TissueTek®, Sakura Finetek Europe B.V., 2408 AV Alphen aan den Rijn, Netherlands)* in embedding cassettes. Air bubbles were removed with a cannula before putting the embedding cassettes into a Styrofoam box with dry ice. The cassettes were stored afterwards in an -80 °C freezer for cryohistological examination.

The following organs were imaged: heart, lung, uterus fat, liver, spleen, pancreas, intestine, kidneys, bladder and additional the mesenterial fat from MCT 415/MCT 416 due to a macroscopic visible tumor.

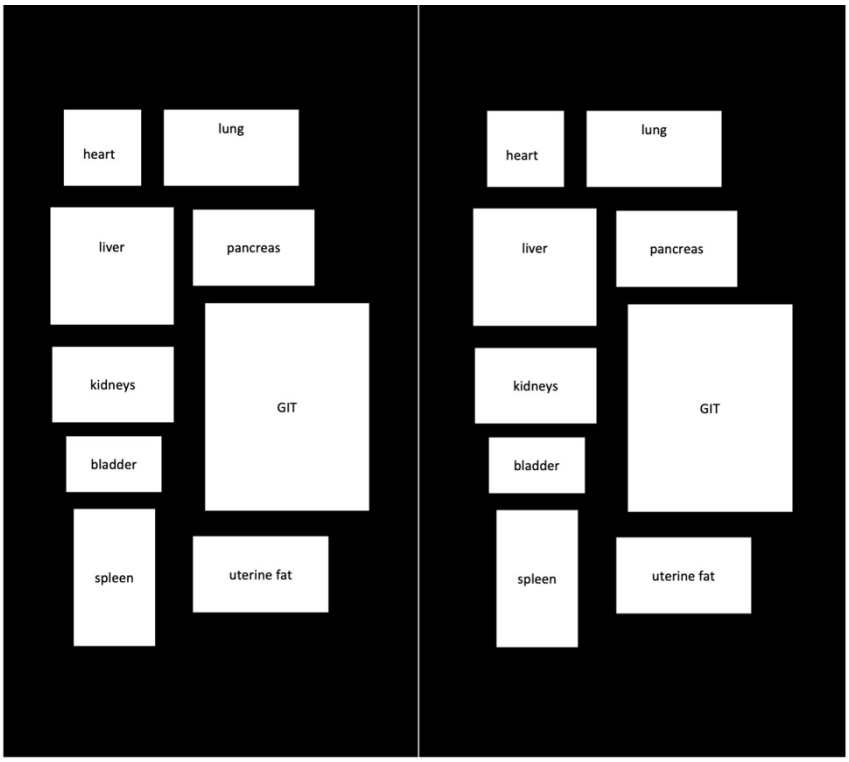

Figure 10 Positioning organs. *The organs were arranged on a black plate, like on the schematic illustration, for the organ imaging session. In each session the organs of two mice were imaged simultaneously, on the right side the organs of the with BGs treated mouse were placed and on the left side the organs from the control animal. Additional in MCT 415 and MCT 416 organ imaging the mesenterial fat was placed under the uterus fat on the black plate.*

3.4 Analysis

The bioluminescence and fluorescence analysis were done by using the Living Image Software *(Living Image® 4.5.2 (64-bit), 128133, compatible with the IVIS Spectrum CT, Perkin Elmer Inc., Waltham, Massachusetts, USA)*. For the evaluation and comparison of the images a region of interest (ROI) was placed over the visual signal. In 2D BLI the ROIs were placed over the thoracic and over the abdominal area to get an overview on the signal strength. In 3D Imaging (FLIT and DLIT) for signal quantification the ROIs were placed directly over the measured signal and in 2D organ imaging (FLI and BLI) over each organ. For detailed information about the image analysis procedure with the Living Image Software see the “Software manual for use with IVIS Spectrum CT” (June 2015) from Perkin Elmer.

4 Results and discussion

4.1 Observation of tumor growth and localization by using bioluminescence imaging

BLI Imaging was used to observe the tumor progression and location after injecting all mice with a luciferase marked colon carcinoma tumor cell line ($CT26^{F\text{-}Luc}$) on day zero. Each mouse received 1 x 10^5 $CT26^{F\text{-}Luc}$ (200 µl) intraperitoneally under a laminar flow hood into the right lower abdomen. Oxaliplatin treatment (6 mg/kg, i.p.), was planned on day three and six of the experiment, but due to slow tumor progression no treatment was necessary.

Due to the less signal intensity, mice were imaged more often than initially planned to observe the tumor progression. The mice were imaged pairwise in supine position on day one, three, six and thirteen in 2D BLI. The signal strength, which grossly correlates with the tumor progression, was quantified by placing regions of interest (ROI) over the thoracic and the abdominal area. The signal was increasing as expected from day one to day thirteen.

Table 9 Measurements of the thoracic and abdominal ROIs. *Increasing Average Radiance [p/s/cm²/sr] values measured in the ROIs placed over the thoracic and the abdominal area from day one, day three, day six and day thirteen from each mouse.*

	Thorax				Abdomen			
	Day 1	Day 3	Day 6	Day 13	Day 1	Day 3	Day 6	Day 13
MCT 351	5,23E+02	6,83E+02	1,92E+03	7,35E+04	1,53E+03	2,99E+03	1,83E+04	1,24E+06
MCT 399	5,21E+02	5,26E+02	1,41E+03	2,98E+05	1,50E+03	6,05E+03	1,53E+05	5,58E+06
MCT 411	7,39E+02	6,07E+02	1,82E+03	9,99E+03	1,69E+03	3,16E+03	9,31E+03	9,07E+05
MCT 414	5,56E+02	4,44E+02	1,02E+03	1,23E+04	6,03E+03	1,29E+04	5,97E+04	1,27E+06
MCT 415	5,64E+02	5,39E+02	4,62E+02	3,17E+03	2,57E+03	2,74E+03	3,38E+03	3,38E+05
MCT 416	4,69E+02	6,38E+02	6,26E+02	1,26E+04	1,78E+03	7,11E+03	5,66E+03	2,16E+06

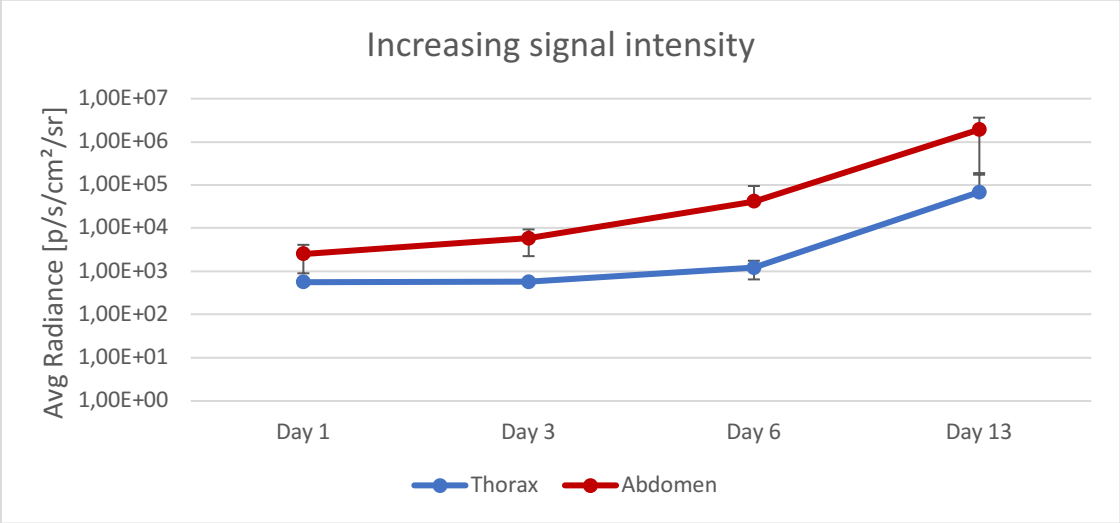

Figure 11 Increasing average radiance after intraperitoneal installation of CT26$^{F\text{-}luc}$ cells. *(Values represent the means ± SD of data obtained from 6 animals)*

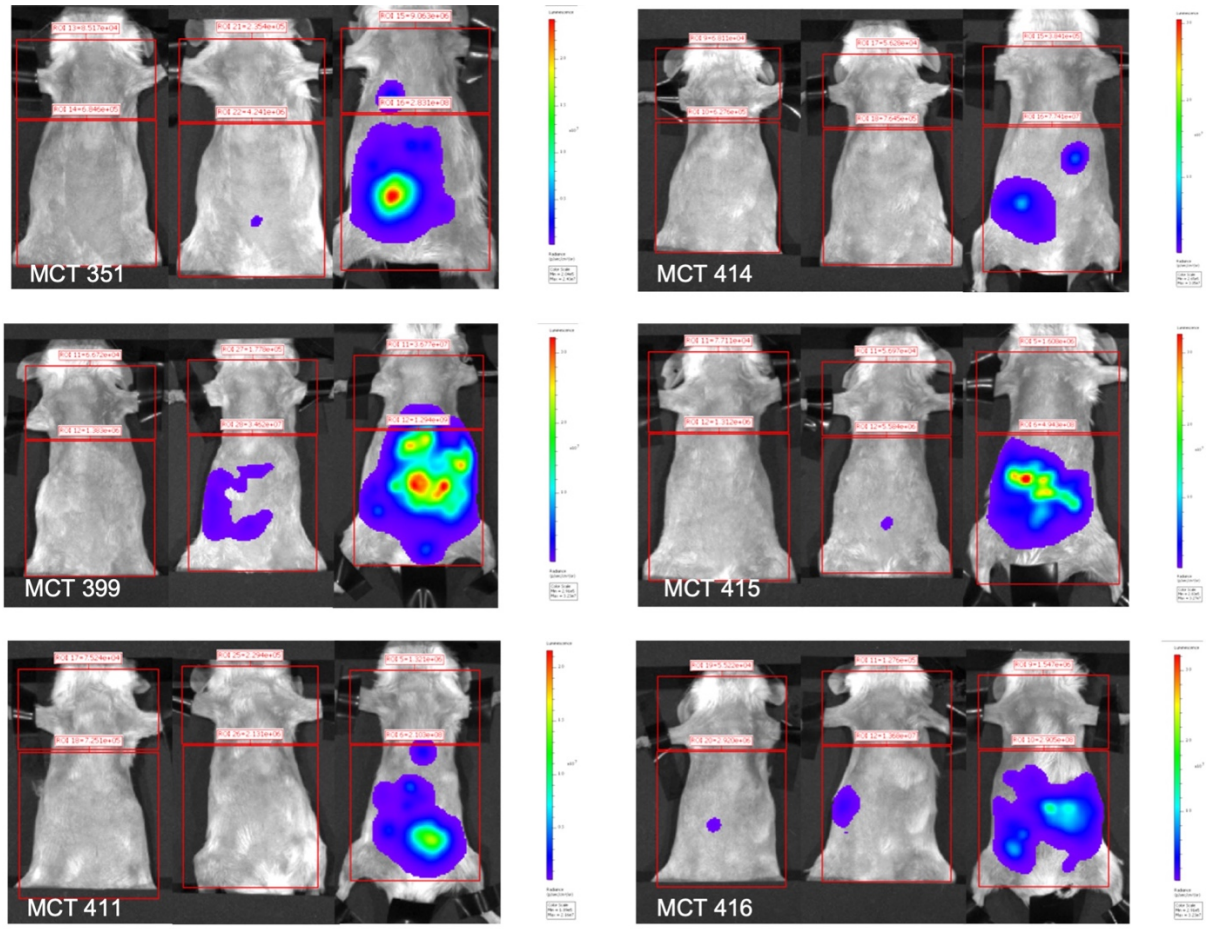

Figure 12 2D BLI Images. *From each animal the 2D bioluminescence image on day three, six and 13 (left to right) are shown. The progression of the luciferase marked colon carcinoma tumor cell line can be observed. The signal in each mouse was mainly located in the abdominal area.*

On day eight and ten every mouse and on day thirteen only mice which have received the bacterial ghosts intraperitoneally were imaged using DLIT/CT to get a more detailed visualization about the tumor size and location. To prevent image overlapping it was necessary to image in DLIT each mouse individually, because during the CT a stack of planar X-ray images from a series of perspectives is reconstructed to a three-dimensional image of the mouse. The settings used are described in the section 3.4.1. Prior the imaging the mice received an iodine-based contrast agent intraperitoneally, to improve the delimitation of the organs in the CT. The signals measured were located in the abdominal area.

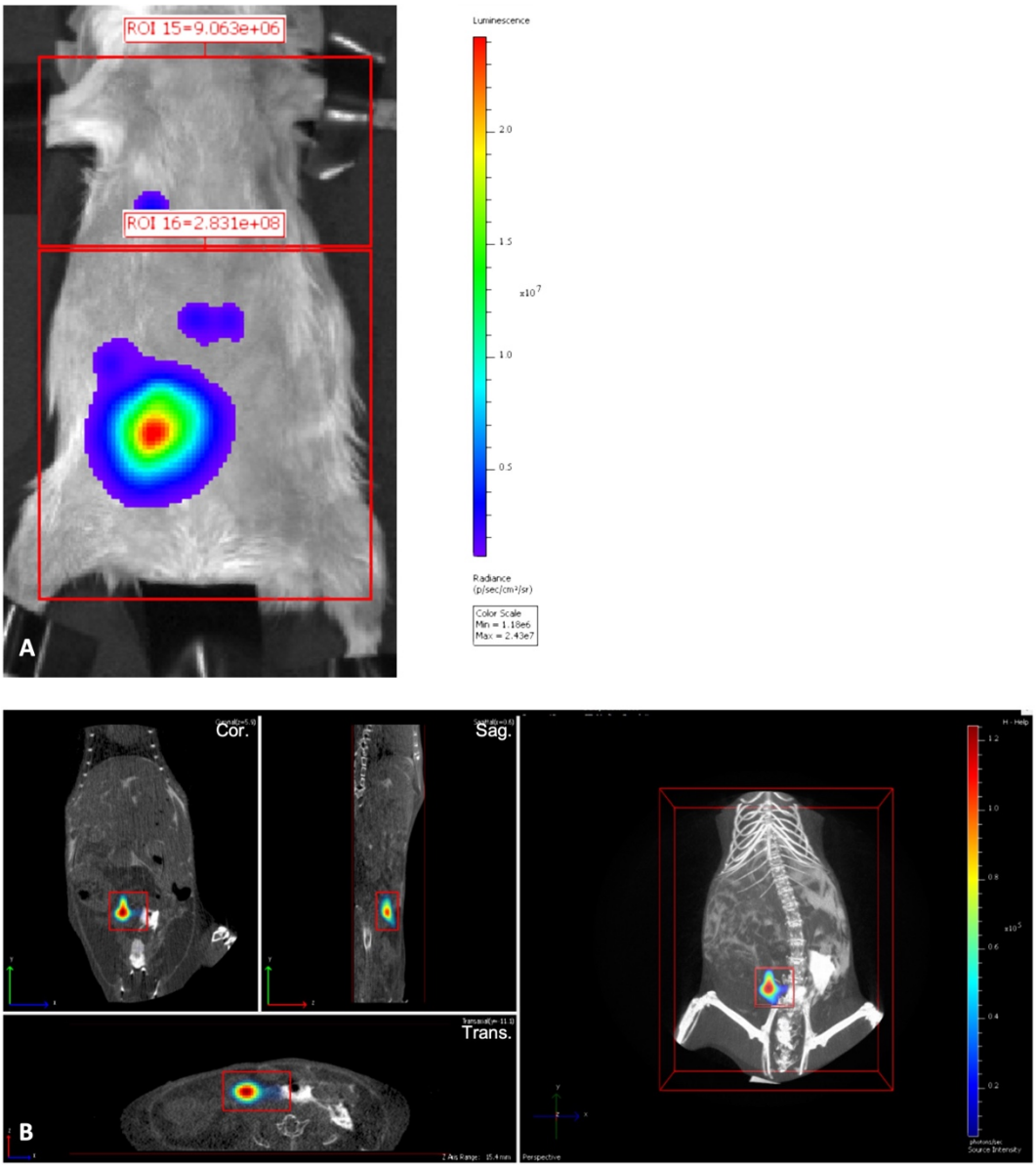

Figure 13 *2D BLI (A) on day 13 and DLIT (B) on day 10 of MCT-351. Cor. = coronal, Sag. = sagittal, Trans. = transaxial*

MCT 351:

In 2D BLI the strongest signal, which was also clearly visible in DLIT was detected in the right lower abdomen at the height of the pelvis entrance (injection area), in the anatomical localization of parts of the gastrointestinal tract, like the small intestine and the colon ascendence. In 2D BLI signals were also detected in the upper abdominal area, anatomically located in this area is the pancreas. (Fig.13)

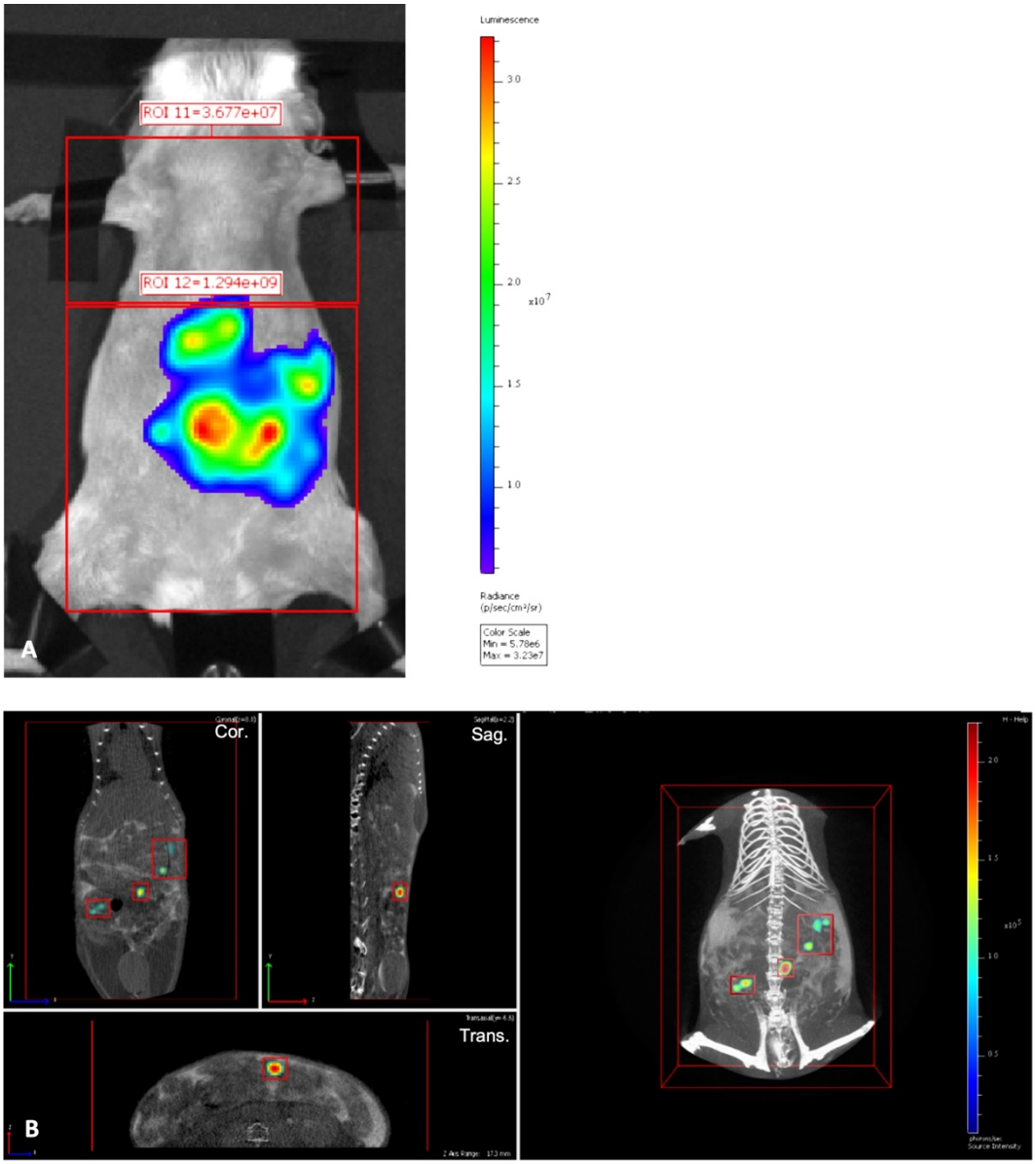

Figure 14 *2D BLI (A) on day 13 and DLIT (B) on day 10 of MCT-399. In the coronal sectional view all three signals are shown. Transaxial and sagittal only the signal located in the abdominal center is pictured. Cor. = coronal, Sag. = sagittal, Trans. = transaxial*

MCT 399:

The strongest DLIT signal was located in the center of the abdomen, probably somewhere in the gastrointestinal tract. A clear allocation to the signal was not possible due to the peristaltic movements of the GIT. In the anatomically localization of parts of the gastrointestinal tract, like the small intestine and the colon ascendence, a second signal, at the right lower abdomen, near the injection area was detected. Another signal was located in the upper left abdominal area, in the anatomical region of the pancreas and the spleen. (Fig. 14)

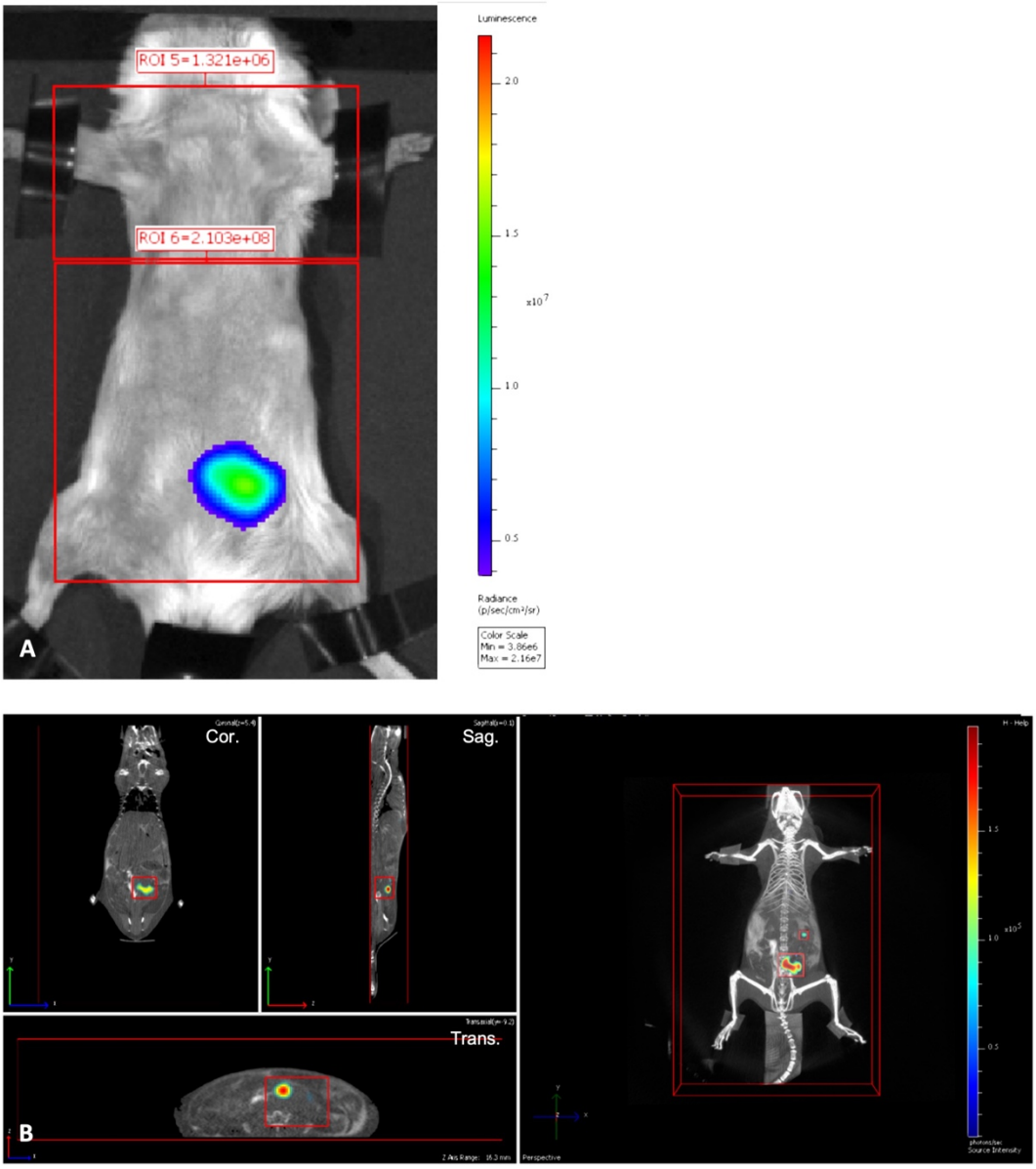

Figure 15 *2D BLI (A) and DLIT (B) of MCT-411 on Day 13. In the coronal, the sagittal and the transaxial sectional view the signal located in the left lower abdomen is illustrated. Cor. = coronal, Sag. = sagittal, Trans. = transaxial*

MCT 411:

The strongest signal was located in the left lower abdomen in 2D BLI and DLIT at the height of the pelvis entrance, in the anatomical localization of parts of the gastrointestinal tract. An additional signal was detected in DLIT in the upper left abdomen, anatomically located in this area is the pancreas and the spleen. (Fig. 15)

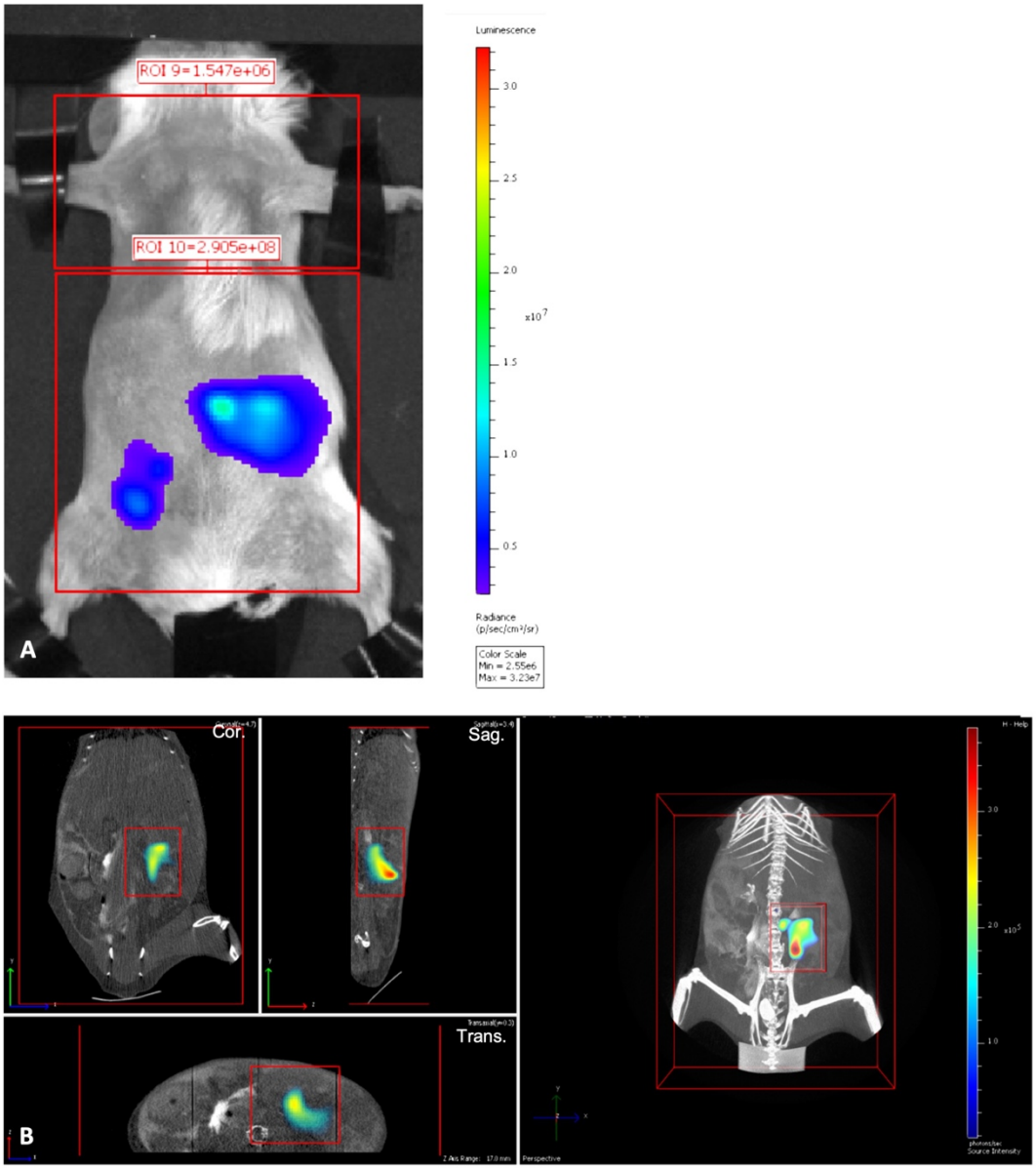

Figure 16 *2D BLI (A) and DLIT (B) of MCT-414 on Day 13. Cor. = coronal, Sag. = sagittal, Trans. = transaxial*

MCT 414:

The strongest signal was located on the left side of the abdomen cranial of the pelvis entrance, presumably located somewhere in the gastrointestinal tract. In 2D BLI a signal was also detected in the right lower abdomen, near the injection area. (Fig. 16)

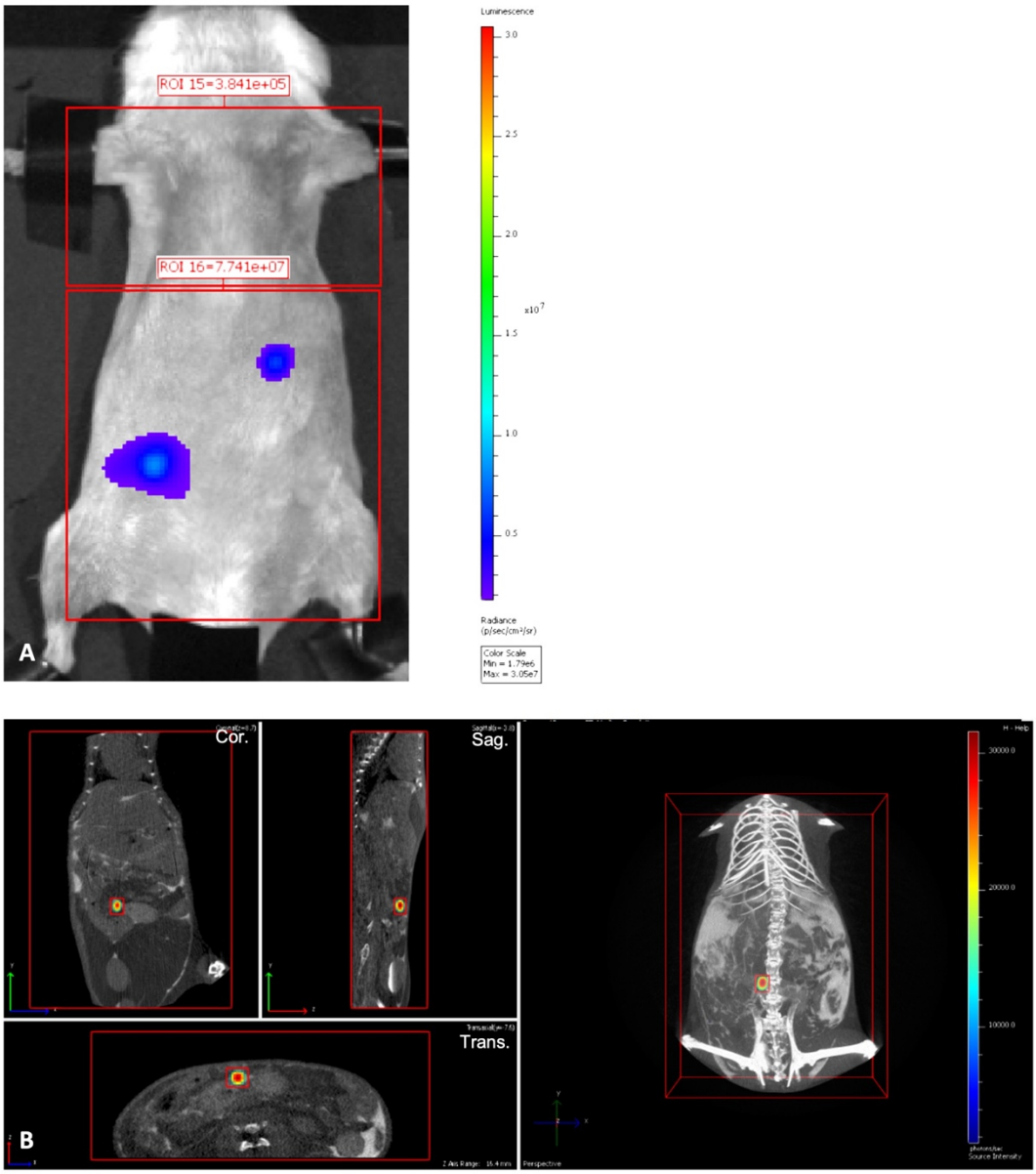

Figure 17 *2D BLI (A) on day 13 and DLIT (B) on day 10 of MCT 415. Cor. = coronal, Sag. = sagittal, Trans. = transaxial*

MCT 415:

In 2D BLI from day 13 the signals were located in the upper left abdomen, in the anatomical localization of the pancreas and the spleen and in the right lower abdomen (injection area), assumedly located somewhere in the gastrointestinal tract. The signal in the right lower abdomen was also detected with DLIT. (Fig. 17)

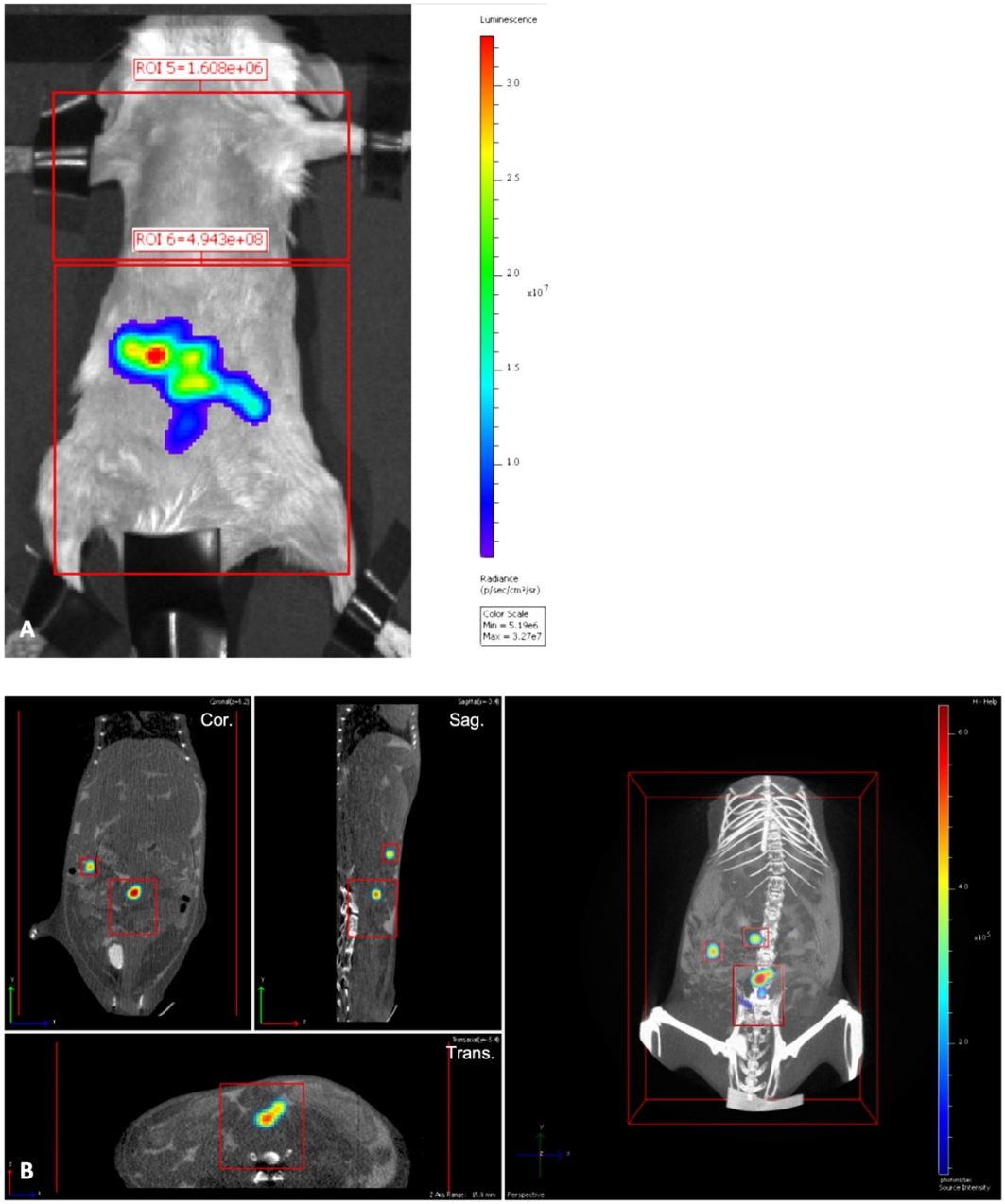

Figure 18 *2D BLI (A) and DLIT (B) of MCT 416 on Day 13. Cor. = coronal, Sag. = sagittal, Trans. = transaxial*

MCT 416:

The signals were distributed over the right lower abdominal side to the center and are probably located within in the gastrointestinal tract. (Fig. 18)

For exact organ allocation of the detected signals a 2D BLI ex vivo organ imaging was performed on day 13 using the settings described in Tab. 7.

After cervical dislocation under anesthesia the organs of the mice were removed and placed on a black plate for ex vivo organ imaging. In every animal the highest signals were measured in the pancreas or in the gastrointestinal tract. A high signal was also seen sometimes in organs like the liver, the spleen or in the uterine fat. The pancreas was in 4 of 6 animals the organ with the highest signal, followed by the gastrointestinal tract. In the remaining two mice the signal in the gastrointestinal tract was a little higher than that of the pancreas. (Tab. 10)

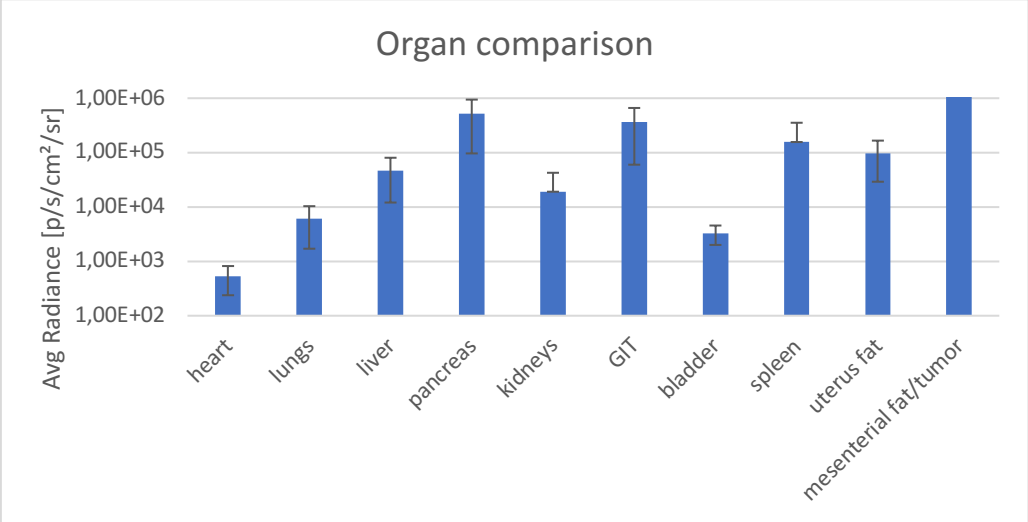

Figure 19 Average radiance of the organs 2D BLI. *After the cervical dislocation the organs were removed and placed on a black plate in a specific order (Fig. 10). 2D bioluminescence imaging was performed using the settings in Tab 7. (Values represent the means ± SD of data obtained from 6 animals) Mesenterial fat/tumor value was measured in MCT 416*

.

Table 10 *Average radiance of the single organs from each mouse.*

	MCT 351	MCT 399	MCT 411	MCT 414	MCT 415	MCT 416
heart	6,35E+02	8,68E+02	9,71E+01	2,11E+02	5,26E+02	8,35E+02
lungs	5,99E+02	1,32E+04	2,55E+03	6,70E+03	3,55E+03	9,56E+03
liver	1,66E+04	4,01E+04	2,93E+03	9,32E+04	3,49E+04	8,97E+04
pancreas	1,84E+04	5,62E+05	4,81E+05	7,75E+05	3,92E+04	1,25E+06

kidneys	2,26E+03	4,13E+04	3,56E+03	4,75E+03	1,47E+03	6,12E+04
GIT	4,34E+04	4,52E+05	6,43E+04	6,01E+05	1,50E+05	8,56E+05
bladder	2,39E+03	3,89E+03	1,93E+03	5,78E+03	3,14E+03	2,56E+03
spleen	1,68E+04	1,22E+05	1,34E+03	5,54E+05	1,70E+03	2,44E+05
uterus fat	1,11E+04	1,33E+05	1,85E+04	7,64E+04	1,49E+05	1,98E+05
mesenterial fat					8,97E+02	1,48E+06

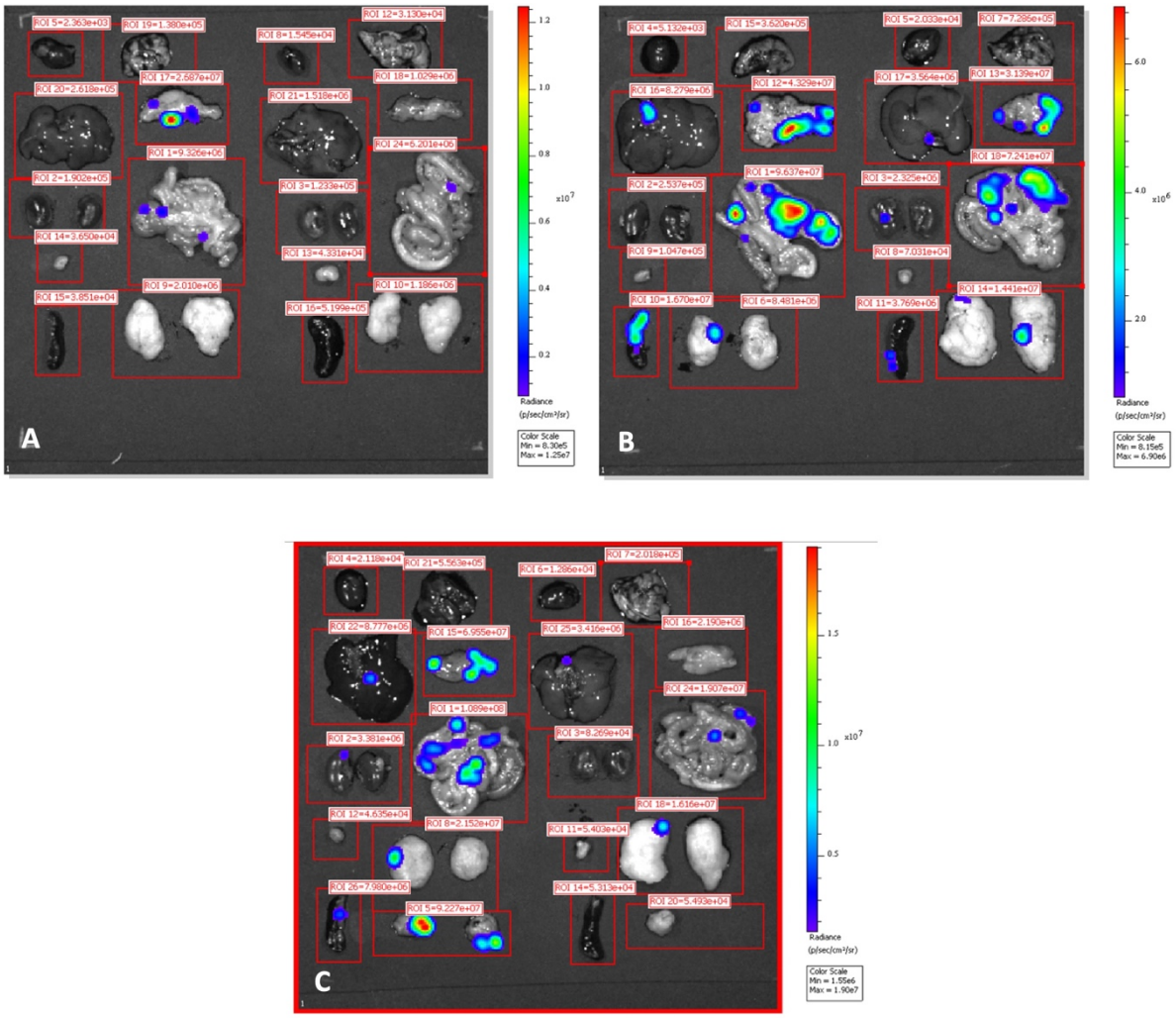

Figure 20 Organ Imaging. *The organs of the control animals were placed on the right side and the organs of the treated animals on the left. The mice were killed pairwise by cervical dislocation, the organs were removed and immediately placed on the black plate in a specific order for imaging (Fig. 10). The signals were mainly located in the pancreas and in the gastrointestinal tract. A MCT 351 (r) MCT 411 (l) / B MCT 399 (r) MCT 414 (l) / C MCT 416 (l) MCT 415 (r)*

4.2 FLI based tracking of bacterial ghost biodistribution in tumor bearing animals

250 µl of the bacterial ghosts, labelled with Alexa Fluor 750 (AF750), were injected with a 1 ml single use insulin syringe intraperitoneally into three mice to examine the biodistribution in tumor bearing animals. In three mice instead of labelled BGs the same amount (250 µl) of 5% Glucose was injected under identical conditions. These mice were used as controls to ensure that the imaging outcomes from the IVIS Spectrum CT are not false positive signals. No control mouse was showing signals in fluorescence imaging, neither *in vivo* nor in *ex vivo*/organ imaging. Two hours after the injection the imaging was performed as described in the section anesthesia and imaging procedure (3.4)

4.2.1 Bacterial ghosts pre signal measurement

A black 96 well plate with labelled BGs, unlabeled BGs and a Buffer (5 % Glucose) was imaged to control if the BGs were labelled correctly with the fluorescent AF750. Each sample was transferred into three wells (100 µl per well) and the black well plate was imaged as described in the section 3.3.

Table 11 Measurements average radiance efficiency 96 well plate. *300 µl of the samples were placed into three different wells (100 µl per well) after vortexing the sample. 2D fluorescence imaging was performed. A ROI was placed over each filled well and over one empty well to measure and compare the signal strengths.*

Avg Radiant Efficiency [p/s/cm²/sr] / [µW/cm²]	
AF750 labeled BG	2,23E+08
AF750 labeled BG	1,97E+08
AF750 labeled BG	1,99E+08
Unlabeled BG	5,81E+05
Unlabeled BG	5,75E+05
Unlabeled BG	6,36E+05
Buffer G 5%	6,46E+05
Buffer G 5%	6,09E+05
Buffer G 5%	5,85E+05
Empty Well	2,84E+05

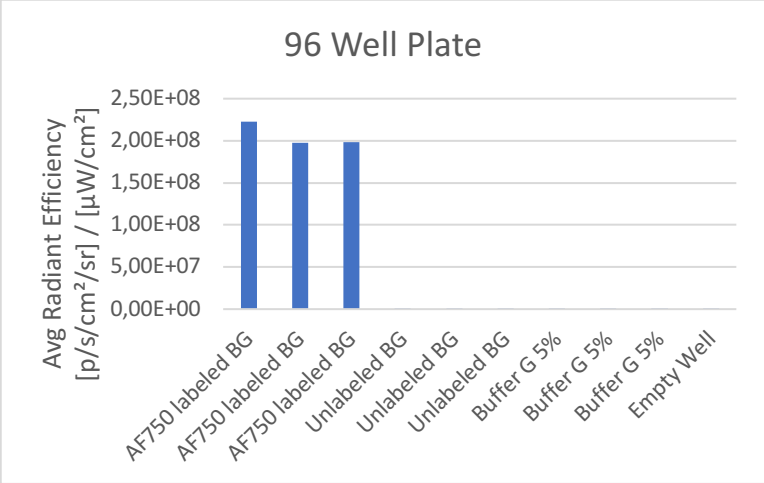

Figure 21 Average radiance efficiency 2D FLI. *A signal was only measured in the wells, where the labeled BGs were placed.*

The average radiant efficiency of the bacterial ghosts labeled with AF750 was between 1,97E+08 and 2,23E+08 (p/s/cm²/sr)/(µW/cm²). Instead, the average radiant efficiencies of the unlabeled BGs, the Buffer (5% Glucose) and the ROI measured in an empty well were between 6,46E+05 and 2,84E+05 (p/s/cm²/sr)/(µW/cm²).

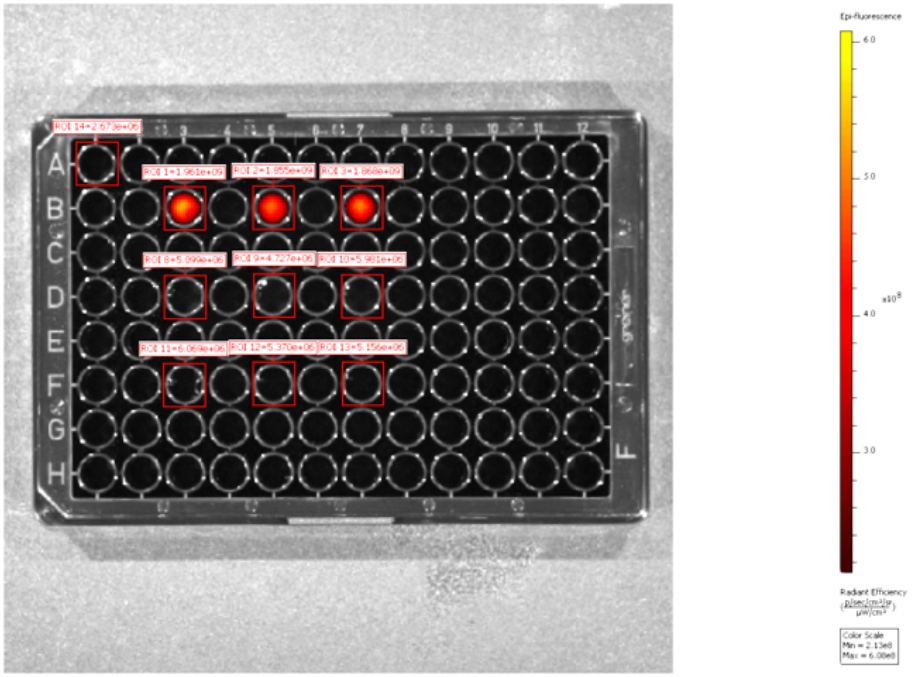

Figure 22 96 Well plate. *The AF750 labeled BGs are located in the wells B3, B5 and B7, the unlabeled BGs in the wells D3, D5 and D7, the buffer (5% Glucose) in the wells F3, F5, F7 and the well A1 was empty and measured for comparison.*

4.2.2 Fluorescence imaging tomography

Two hours after the intraperitoneal application of AF750 labeled bacterial ghosts the imaging session described in Fig. 9 was started. For the FLIT each mouse from the treated group was imaged individually as described in the section Fluorescence imaging (3.4.2).

The detected signals were all located in the abdominal area. In each animal signals were measured in areas were anatomical located are the pancreas, the urinary bladder and in 2 of 3 mice also in the gastrointestinal tract. The signal in the urinary bladder probably occurs from renal excretion after degradation of BGs.

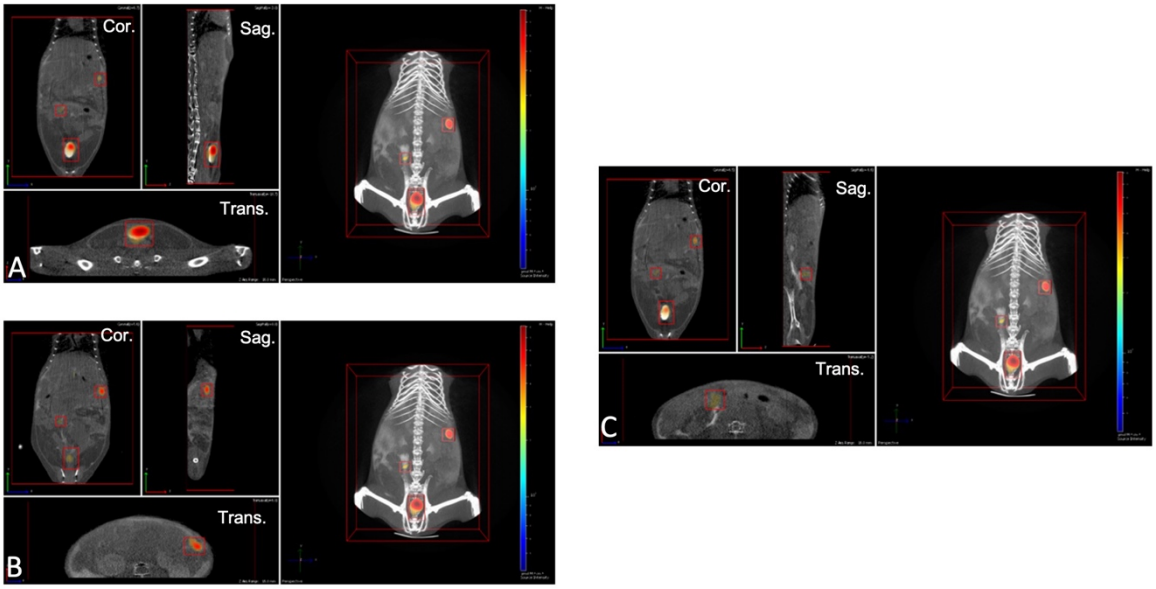

Figure 23 *FLIT/CT MCT 411 on Day 13. A Signal bladder, B Signal pancreas, C Signal GIT / Cor. = coronal, Sag. = sagittal, Trans. = transaxial*

<u>MCT 411:</u>

The strongest signals were located in the upper left abdomen, in the anatomical localization of the pancreas and the spleen, somewhere in the gastrointestinal tract and in the region of the urinary bladder.

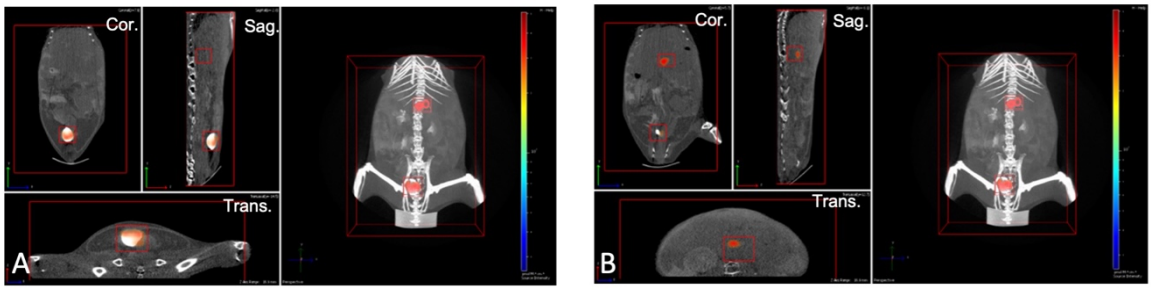

Figure 24 *FLIT/CT MCT 414 on Day 13. A Signal bladder, B Signal pancreas / Cor. = coronal, Sag. = sagittal, Trans. = transaxial*

MCT 414:

The signals were measured in the upper abdominal area, in the anatomical localization of in the pancreas and in the region of the urinary bladder.

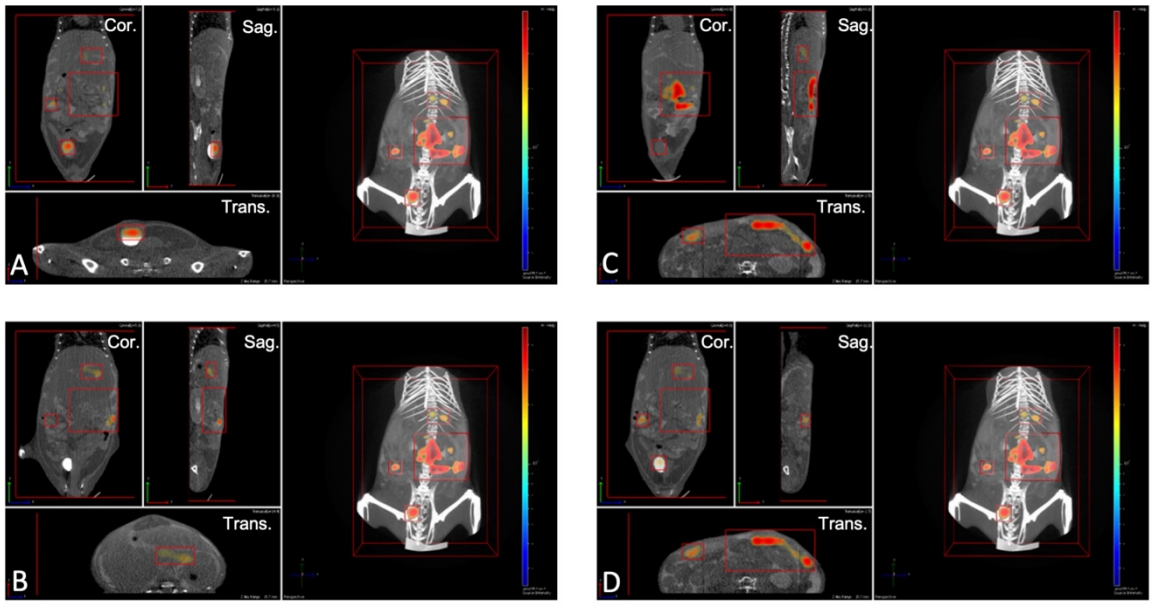

Figure 25 *FLIT/CT MCT 416 on Day 13. A Signal bladder, B Signal pancreas, C Signal GIT (extending from the abdominal center to the left side), D Signal GIT (right lower abdomen) / Cor. = coronal, Sag. = sagittal, Trans. = transaxial*

MCT 416:

The signal in the upper abdomen was located in the area of the pancreas. The signal at the right lower abdomen and the signal extending from the center to the left side, are presumably

located in the gastrointestinal tract. A signal was also located near the anatomical localization of the urinary bladder.

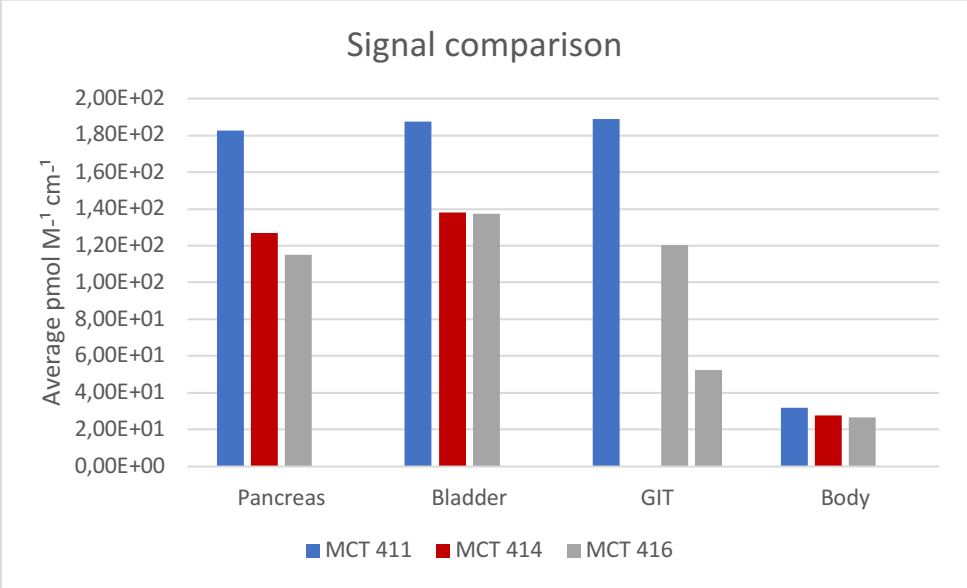

***Figure 26 Average pmol M-¹ cm-¹ signal comparison**. In MCT 416 two signals located in the GIT were detected, one in the right lower abdomen and the other one extending from the abdominal center to the left side. The average pmol M-¹ cm-¹ of the signal extending from the abdominal center to the left side from MCT 416 was lower than that of the other signals, due to the big size of the ROI.*

***Table 12 Average pmol M-¹ cm-¹ ROI Measurements**. The mean average pmol M-¹ cm-¹ of the signals in the gastrointestinal tract was 1,21E+02, from signals measured near the pancreas 1,42E+02 and from signals in the bladder 1,54E+02. The mean body average pmol M-¹ cm-¹ was 2,88E+01.*

	Pancreas	Bladder	GIT		Body
MCT 411	1,83E+02	1,88E+02	1,89E+02		3,21E+01
MCT 414	1,27E+02	1,38E+02			2,78E+01
MCT 416	1,15E+02	1,38E+02	1,20E+02	5,26E+01	2,66E+01

Due to the stopped Gastrografin treatment and the medium resolution micro-CT a precise organ allocation in the FLIT/CT images was not possible. For the exact organ allocation a 2D FLI ex vivo organ imaging was performed after the cervical dislocation under anesthesia using the settings described in Tab. 8.

4.2.3 2D FLI organ imaging

Analysis was done by spectral unmixing, which allows to extract the signal from the fluorophore (AF750) from the tissue autofluorescence. (PerkinElmer Health Sciences 2017) As expected, the organs from the control group have not shown any signal. The strongest signal in each mouse from the treated group was observed in the pancreas. A strong signal was also measured in the gastrointestinal tract.

In the bladder at the ex vivo organ imaging in contrast to the FLIT/CT no signal was detected. The BGs measured could have been in the urine, due to renal excretion. During the killing and preparation process the bladder was emptied, which could be the reason why no high signal was measured in the urinary bladder. It could also be that the AF750 was degraded very quickly and therefore it was no longer possible to measure a signal.

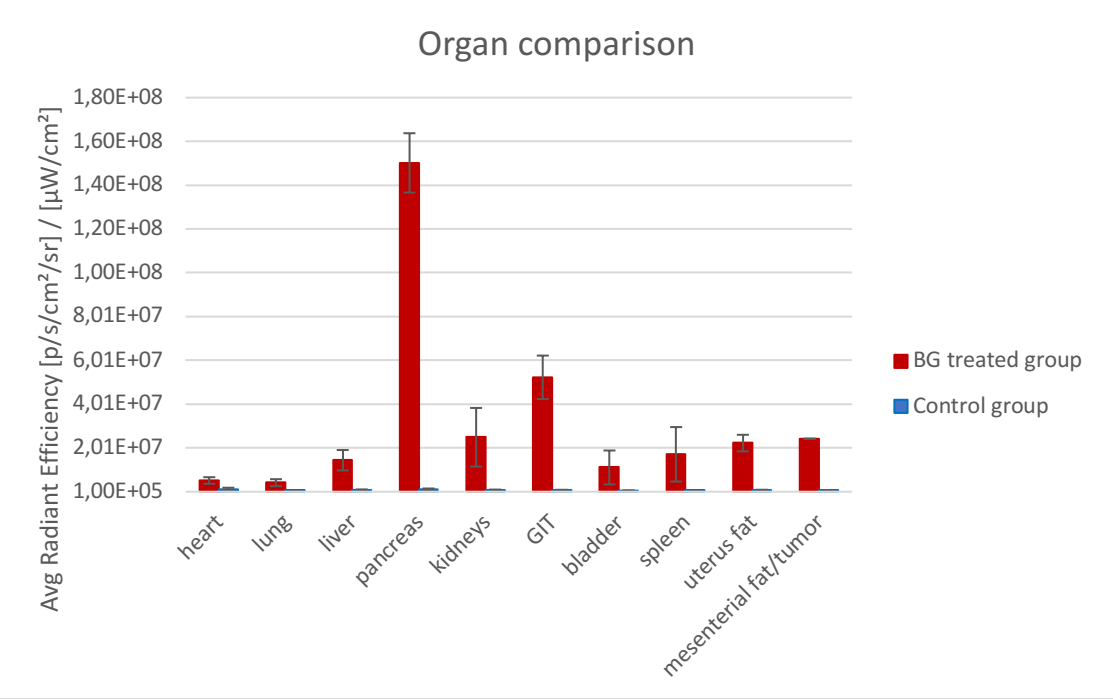

Figure 27 Average radiant efficiency organ comparison. *Treated vs. Control. (Values represent the means ± SD of data obtained from 3 animals) Here a clear signal in the pancreatic tissue is visible.*

Table 13 2D FLI ex vivo organ ROI Measurements *(Average radiant efficiency). (Values represent the means ± SD of data obtained from 3 animals)*

	BG treated group	Control group
heart	5,22E+06	1,23E+06
lung	4,22E+06	6,53E+05
liver	1,45E+07	9,00E+05
pancreas	**1,50E+08**	1,22E+06
kidneys	2,49E+07	8,25E+05
GIT	5,23E+07	6,90E+05
bladder	1,12E+07	5,68E+05
spleen	1,72E+07	7,32E+05
uterus fat	2,23E+07	6,81E+05
mesenterial fat/tumor	2,43E+07	8,25E+05

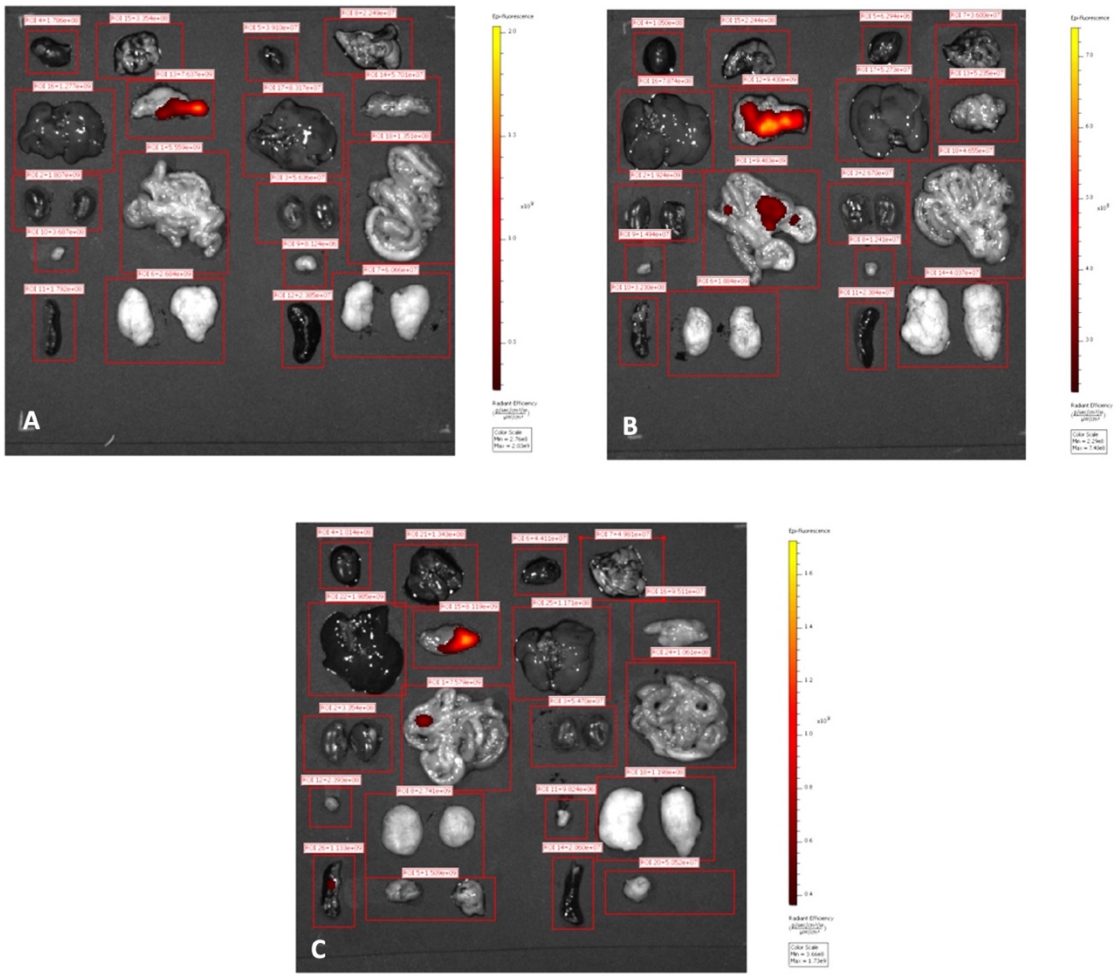

Figure 28 2D FLI organ imaging. *The organs of the control animals were placed on the right side and the organs of the BG treated mice on the left.) The organs are placed as described in Fig. 10. As expected, no signals occurred in the organs from the control group. The organs with the strongest signals were the pancreas and the gastrointestinal tract. (A: MCT 351 (r) MCT 411 (l) / B: MCT 399 (r) MCT 414 (l) / C: MCT 416 (l) MCT 415 (r))*

4.3 Association of bacterial ghosts to tumor regions

It was recently shown that the addition of BGs to oxaliplatin enhances the immunogenic cell death of cancer cells in vitro (CRC line CT26) and that in peritoneal carcinomatosis models (BALB/c) *in vivo* the treatment combination has a significant antitumor activity, for the reason that BGs are highly immune-stimulating and oxaliplatin is dependent on an activate immune system. (Groza et al. 2018) As mentioned before BGs are in addition able to deliver proteins, pharmaceuticals, antigens and nucleic acids, so if the bacterial ghosts have a tumor associated biodistribution, they could transport the cytotoxic substances for therapy directly to the tumors. (Ganeshpurkar et al. 2014)
A large number of side effects are occurring when cytotoxic anticancer agents are used for therapy. (Ganeshpurkar et al. 2014) The side effects could be reduced if the substances were transported and used directly at the tumor localization rather than systemically.

To observe the tumor association 2D BLI and 2D FLI ex vivo organ images of every treated mouse are compared. (Fig 30, Fig. 31, Fig. 32)

The bacterial ghosts distribute mainly in the pancreas and in the gastrointestinal tract. In MCT 411 the bacterial ghosts were located in the pancreas, near to the tumor area. In MCT 414 the bacterial ghosts were visible in regions in the pancreas and in the gastrointestinal tract, where also tumors are located. In MCT 416 BGs were located in tumor regions in the pancreas, the spleen and the gastrointestinal tract, but in the mesenterial fat where a macroscopic visible tumor was detected no bacterial ghosts were measured.

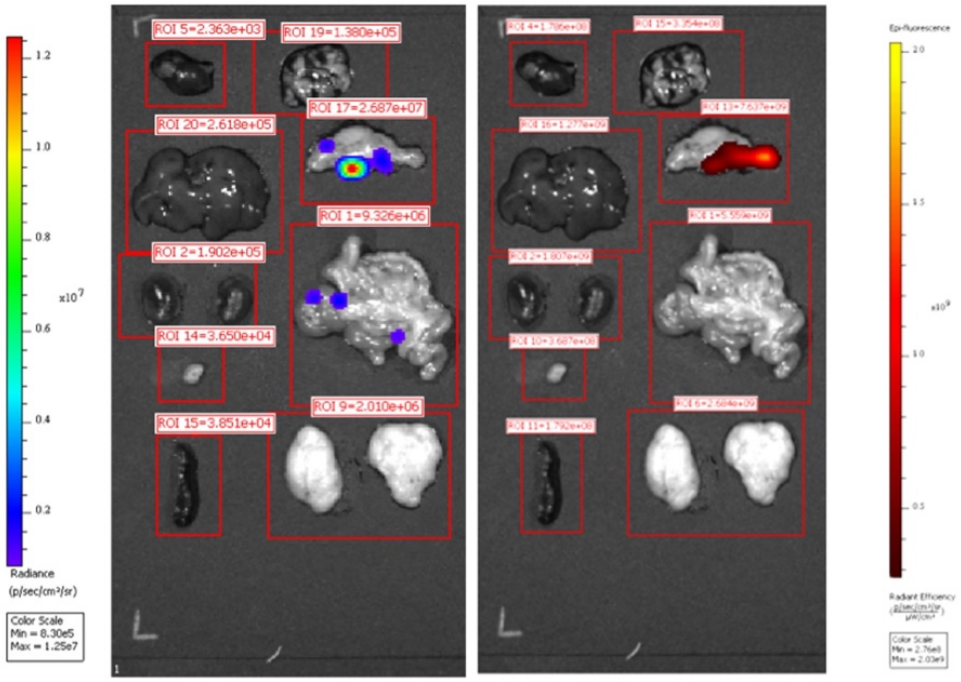

Figure 29 2D BLI (l) and 2D FLI (r) ex vivo organ imaging MCT 411. *In the bioluminescence image the CT26 cancer cells and in the fluorescence image the AF750 labeled BGs are shown. In the pancreas the bacterial ghosts were located near the region were the tumor (shown in BLI) is located.*

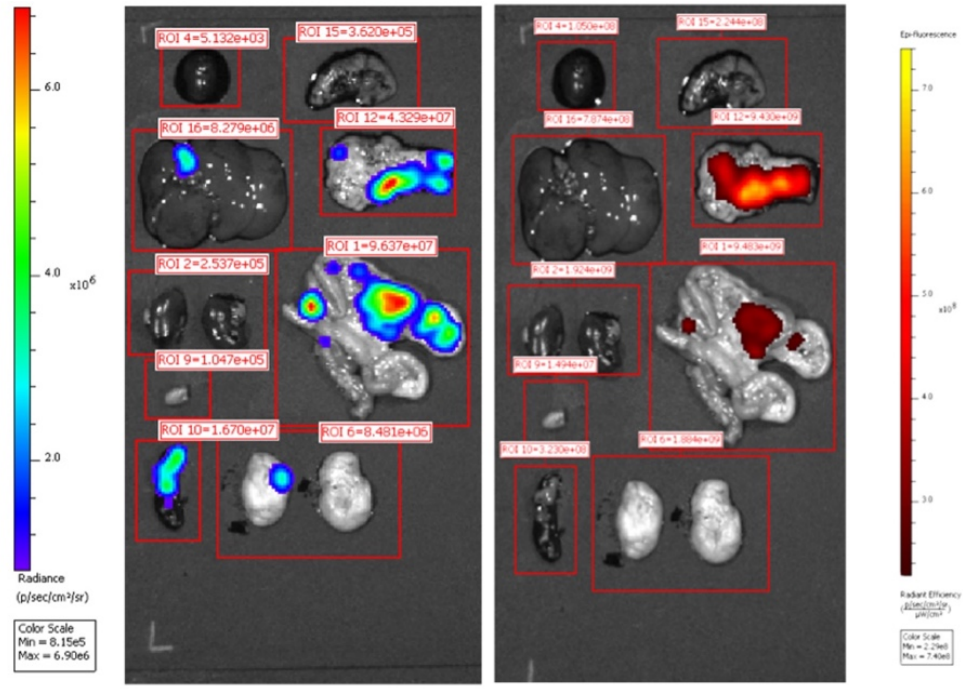

Figure 30 2D BLI (l) and 2D FLI (r) ex vivo organ imaging MCT 414. *In the bioluminescence image the CT26 cancer cells and in the fluorescence image the AF750 labeled BGs are shown. If the images are compared, it is visible that the bacterial ghosts in FLI were located in tumor regions (visible in BLI) in the pancreas and in the gastrointestinal tract.*

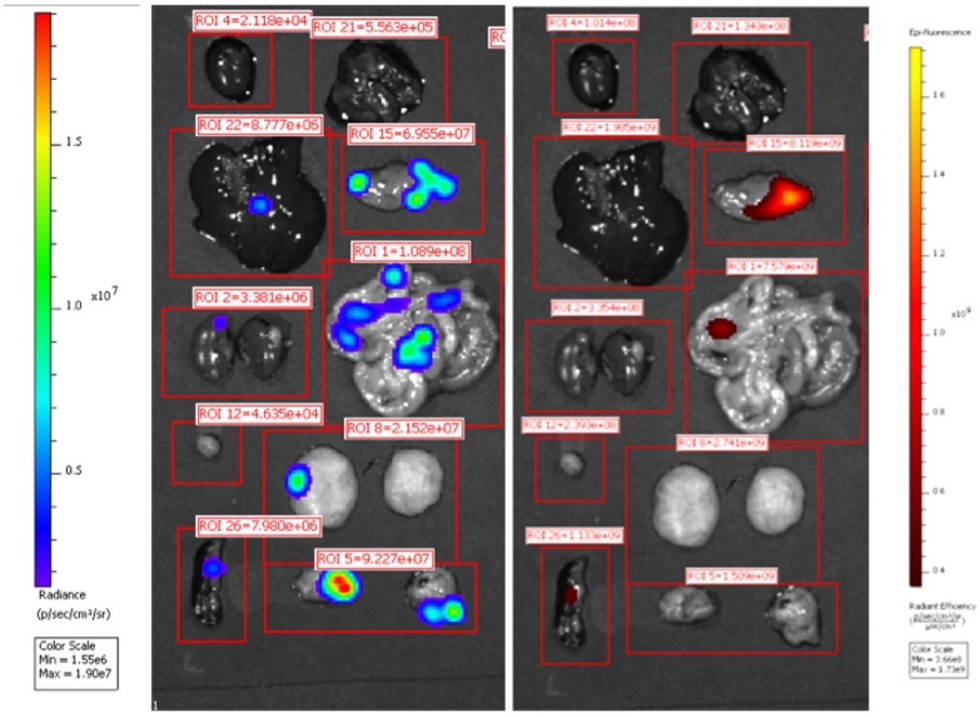

Figure 31 2D BLI (l) and 2D FLI (r) ex vivo organ imaging MCT 416. *In the bioluminescence image the CT26 cancer cells and in the fluorescence image the AF750 labeled BGs are shown. It is visible that the bacterial ghosts in FLI were located in tumor areas (visible in BLI) in the pancreas, the spleen and the gastrointestinal tract. No bacterial ghosts were detected in the region of the tumor with the strongest signal in the mesenterial fat.*

The images show that bacterial ghosts are distributing towards tumor regions. A cryohistological examination has to verify if the BGs are directly associated to the tumors.

5 Conclusion

In this diploma thesis fluorescence and bioluminescence imaging in combination with μCT were used for a biodistribution study in a tumor bearing animal model to investigate if bacterial ghosts are distributing in a tumor-associated manner and could therefore be considered as drug carriers of cytotoxic substances for tumor therapy. Bioluminescence imaging was used to observe the tumor progression and localization and fluorescence imaging to study the biodistribution of the macromolecular drug carrier (BGs). Therefore, the animals were imaged approximately two hours after the intraperitoneal installation of AF750 labeled BGs using 2D FLI, FLIT/CT and ex vivo organ epifluorescence imaging. The BGs were mainly detected in the pancreas and the gastrointestinal tract, in organs, where also the highest tumor signals were measured.

With FLIT/CT it was possible to define the region and to assume the organ, in which the signal from the labeled BGs occurred, but a precise organ allocation and correlation to tumors with FLIT/CT was not possible in this study. The anatomical structures were not clearly definable, partly due to the medium resolution of the micro-CT and in addition the oral Gastrografin treatment had to be stopped, because the mice showed behavioral abnormalities during/after the application, which inhibited a reliable signal allocation to the gastrointestinal tract. The ex vivo organ images were better suited to correlate signals (BLI and FLI) with specific organs and in addition a direct comparison of the 2D BLI and the 2D FLI ex vivo organ images showed that the AF750 labeled bacterial ghosts are distributing towards tumor regions.

The organs were embedded in TissueTek and stored in a -80°C freezer for cryohistological examination to validate the *in vivo* imaging results and to verify if the BGs are directly associated to the tumors.

6 Abstract

In vivo imaging is a very important tool towards the principle of 3R. By using *in vivo* optical imaging techniques preclinical biodistribution studies are possible, which are essential for drug development. Optical imaging is used to obtain molecular and functional information by using fluorescence imaging (FLI) or bioluminescence imaging (BLI). FLI uses molecules with specific excitation an emission wavelength, they need to get excited from an external light source to emit photons. BLI uses molecules which act as a light source, they can emit photons due to an enzymatic catalyzed reaction. Labelling with fluorochromes allows to track the spatiotemporal distribution using fluorescence imaging. Bioluminescence imaging (BLI) enables longitudinal monitoring of disease processes in the same animal, for example to observe tumor cell growth of modified cancer cells. The combination of optical imaging with computed tomography enables additionally an anatomical allocation of the signals measured with BLI and FLI.

In this project the BLI tool was used for the observation of the tumor progression and localization and FLI to observe the biodistribution of a macromolecular drug carrier (bacterial ghosts) in a mouse model *in vivo*. The modified CT26 cells were intraperitoneally injected in BALB/c mice causing tumors in the peritoneal cavity with the tendency to colonize the pancreatic area. The bacterial ghosts were labeled with the fluorophore Alexa Fluor 750 (AF750). The labeled BGs were injected intraperitoneally into the tumor bearing animals and their biodistribution was studied by using 2D epifluorescence imaging and fluorescent Imaging tomography. In the ex vivo organ images a precise organ allocation and a signal correlation to tumor regions was possible. The AF750 labeled BGs were mainly detected in the pancreas and the gastrointestinal tract, in organs, where also the highest tumor signals were measured. This data indicates that BGs are distributing in a tumor-associated manner and can therefore be considered as drug carriers of cytotoxic substances for tumor therapy. The organs were stored for cryohistological examination to validate the *in vivo* imaging data results.

7 Zusammenfassung

Die In-vivo-Bildgebung ist ein sehr wichtiges Instrument im Hinblick auf das Prinzip der 3R. Durch den Einsatz optischer Bildgebung sind präklinische Bioverteilungsstudien möglich, die für die Arzneimittelentwicklung unerlässlich sind. Die optische Bildgebung wird eingesetzt um molekulare und funktionelle Informationen mit Hilfe der Fluoreszenzbildgebung (FLI) oder der Biolumineszenzbildgebung (BLI) zu erhalten. FLI verwendet fluoreszierende Farbstoffe mit spezifischen Anregungs- und Emissionswellenlängen, die von einer externen Lichtquelle angeregt werden und dadurch Photonen emittieren. In der BLI werden Photone gemessen, welche bei einer enzymatischen katalysierten Reaktion von Enzymen (Luciferasen) mit ihren Substraten entstehen. Die Markierung von spezifischen Vehikeln wie z.B. von Bacterial Ghosts, mit fluoreszierenden Farbstoffen ermöglicht es, deren räumliche und zeitliche Verteilung mittels Fluoreszenzbildgebung zu verfolgen. Die Biolumineszenz-Bildgebung (BLI) ermöglicht eine longitudinale Beobachtung von Krankheitsgeschehnissen im selben Tier wie z.B. die Beobachtung des Tumorzellwachstums von modifizierten Krebszellen. Die Kombination der optischen Bildgebung mit der Computertomographie ermöglicht die Darstellung der mit BLI und FLI gemessenen Signale in einem anatomischen Zusammenhang. In diesem Projekt wurde die BLI Bildgebung zur Beobachtung der Tumorprogression und -lokalisierung und FLI zur Beobachtung der Biodistribution eines makromolekularen Arzneistoffträger Systems (BGs) in einem Mausmodell *in vivo* eingesetzt. Die modifizierten CT26-Zellen wurden in BALB/c-Mäusen intraperitoneal injiziert und verursachten Tumore in der Peritonealhöhle mit der Tendenz zur Besiedlung des Pankreasbereichs. Die Bacterial Ghosts wurden mit dem Fluorophor Alexa Fluor 750 (AF750) markiert und anschließend intraperitoneal in die tumortragenden Tiere injiziert, um die Bioverteilung zu verfolgen. Dazu wurde die 2D-Epifluoreszenzbildgebung und fluoreszierende Bildgebungstomographie verwendet. In den ex vivo Organbildern war eine genaue Zuordnung der Signale zu Organen und eine Signalkorrelation zu den Tumoren möglich. Die AF750-markierten BGs wurden hauptsächlich in der Bauchspeicheldrüse und im Magen-Darm-Trakt nachgewiesen, meist in Verbindung zu Tumorregionen.

Die in diesem Experiment erhaltenen Daten deuten darauf hin, dass sich die BGs tumorassoziiert verteilen, sie könnten sich deshalb gut als Arzneistoffträger System für den Transport von zytotoxischen Substanzen zur Tumortherapie eignen. Die Organe wurden für kryohistologische Untersuchungen eingelagert, um die Ergebnisse der In-vivo-Bildgebung zu validieren.

Abbreviations

AF750	AlexaFluor750
AMP	Adenosine monophosphate
ATP	Adenosine triphosphate
BGs	Bacterial Ghosts
BLI	Bioluminescence Imaging
CCD	Charge-coupled device
CT	Computed tomography
CT26	Murine colorectal carcinoma cell line
DLIT	Diffuse Luminescence Imaging Tomography
GIT	Gastrointestinal tract
FLI	Fluorescence Imaging
FLIT	Fluorescent Imaging tomography
F-Luc	Firefly luciferase
IVIS	*In vivo* imaging system
OI	Optical Imaging
SPF	Specific-pathogen-free
ROI	Region of Interest

References

Arms L, Robson A-L, Woldu A, Martin A, Palmer W, Flynn J, Hua S. 2020. Considerations for using optical clearing techniques for 3D imaging of nanoparticle biodistribution. International Journal of Pharmaceutics, 588:119739.

Badr CE, Tannous BA. 2011. Bioluminescence imaging: progress and applications. Trends in Biotechnology, 29(12):624–633.

Bashore T. 2001. Fundamentals of x-ray imaging and radiation safety. Catheterization and Cardiovascular Interventions, 54(1):126–135.

Castle JC, Loewer M, Boegel S, de Graaf J, Bender C, Tadmor AD, Boisguerin V, Bukur T, Sorn P, Paret C, et al. 2014. Immunomic, genomic and transcriptomic characterization of CT26 colorectal carcinoma. BMC Genomics, 15(1).

Condeelis J, Weissleder R. 2010. In Vivo Imaging in Cancer. Cold Spring Harbor Perspectives in Biology, 2(12).

De Angelis I, Ricceri L, Vitale A. 2019. The 3R principle: 60 years taken well. Preface. Annali dell'Istituto Superiore Di Sanita, 55(4):398–399.

Etrych T, Lucas H, Janoušková O, Chytil P, Mueller T, Mäder K. 2016. Fluorescence optical imaging in anticancer drug delivery. Journal of Controlled Release, 226:168–181.

Frangioni JV. 2003. In vivo near-infrared fluorescence imaging. Current Opinion in Chemical Biology, 7(5):626–634.

Ganeshpurkar A, Ganeshpurkar A, Pandey V, Agnihotri A, Bansal D, Dubey N. 2014. Harnessing the potential of bacterial ghost for the effective delivery of drugs and biotherapeutics. International Journal of Pharmaceutical Investigation, 4(1):1–4.

Geyer A, Lorenzer C, Gehrig S, Simlinger M, Winkler J, Sami H, Ogris M. 2017a. Fluorescence- and computed tomography for assessing the biodistribution of siRNA after intratracheal application in mice. International Journal of Pharmaceutics, 525(2):359–366.

Geyer A, Taschauer A, Alioglu F, Anton M, Maier J, Drothler E, Simlinger M, Yavuz S, Sami H, Ogris M. 2017b. Multimodal Fluorescence and Bioluminescence Imaging Reveals Transfection Potential of Intratracheally Administered Polyplexes for Breast Cancer Lung Metastases. Human Gene Therapy, 28(12):1202–1213.

Greer LF, Szalay AA. 2002. Imaging of light emission from the expression of luciferases in living cells and organisms: a review. Luminescence, 17(1):43–74.

Groza D, Gehrig S, Kudela P, Holcmann M, Pirker C, Dinhof C, Schueffl HH, Sramko M, Hoebart J, Alioglu F, et al. 2018. Bacterial ghosts as adjuvant to oxaliplatin chemotherapy in colorectal carcinomatosis. Oncoimmunology, 7(5).

Hindelang F, Zurbach R, Roggo Y. 2015. Micro Computer Tomography for medical device and pharmaceutical packaging analysis. Journal of Pharmaceutical and Biomedical Analysis, 108:38–48.

Key J, Leary JF. 2014. Nanoparticles for multimodal in vivo imaging in nanomedicine. International Journal of Nanomedicine, 9:711–726.

Kudela P, Koller VJ, Lubitz W. 2010. Bacterial ghosts (BGs)—Advanced antigen and drug delivery system. Vaccine, 28(36):5760–5767.

Kunjachan S, Gremse F, Theek B, Koczera P, Pola R, Pechar M, Etrych T, Ulbrich K, Storm G, Kiessling F, et al. 2013. Non-Invasive Optical Imaging of Nanomedicine Biodistribution. ACS nano, 7(1):252–262.

Langemann T, Koller VJ, Muhammad A, Kudela P, Mayr UB, Lubitz W. 2010. The bacterial ghost platform system. Bioengineered Bugs, 1(5):326–336.

Lauber DT, Fülöp A, Kovács T, Szigeti K, Máthé D, Szijártó A. 2017. State of the art in vivo imaging techniques for laboratory animals. Laboratory Animals, 51(5):465–478.

Leblond F, Davis SC, Valdés PA, Pogue BW. 2010. Preclinical Whole-body Fluorescence Imaging: Review of Instruments, Methods and Applications. Journal of photochemistry and photobiology. B, Biology, 98(1):77–94.

Li S, Ruan Z, Zhang H, Xu H. 2021. Recent achievements of bioluminescence imaging based on firefly luciferin-luciferase system. European Journal of Medicinal Chemistry, 211:113111.

Manni I, de Latouliere L, Gurtner A, Piaggio G. 2019. Transgenic Animal Models to Visualize Cancer-Related Cellular Processes by Bioluminescence Imaging. Frontiers in Pharmacology, 10.

Moreno MJ, Ling B, Stanimirovic DB. 2020. In vivo near-infrared fluorescent optical imaging for CNS drug discovery. Expert Opinion on Drug Discovery, 15(8):903–915.

Müller J, Wunder A, Licha K. 2013. Optical imaging. Recent Results in Cancer Research. Fortschritte Der Krebsforschung. Progres Dans Les Recherches Sur Le Cancer, 187:221–246.

Paukner S, Stiedl T, Kudela P, Bizik J, Laham FA, Lubitz W. 2006. Bacterial ghosts as a novel advanced targeting system for drug and DNA delivery. Expert Opinion on Drug Delivery, 3(1):11–22.

PerkinElmer Health Sciences, 2012. IVIS Spectrum CT User Manual.

PerkinElmer Health Sciences, 2017. Software Manual for use with IVIS Spectrum.

Peterson NC, Wilson GG, Huang Q, Dimasi N, Sachsenmeier KF. 2016. Biodistribution Analyses of a Near-Infrared, Fluorescently Labeled, Bispecific Monoclonal Antibody Using Optical Imaging. Comparative Medicine, 66(2):90–99.

Rawson SD, Maksimcuka J, Withers PJ, Cartmell SH. 2020. X-ray computed tomography in life sciences. BMC Biology, 18.

Sato A, Klaunberg B, Tolwani R. 2004. In Vivo Bioluminescence Imaging. Comparative Medicine, 54(6):631–634.

Sharifian S, Homaei A, Hemmati R, B. Luwor R, Khajeh K. 2018. The emerging use of bioluminescence in medical research. Biomedicine & Pharmacotherapy, 101:74–86.

Tseng J-C, Vasquez K, Peterson JD. 2017. Optical Imaging on the IVIS SpectrumCT System: General. 18.

Weitz J, Koch M, Debus J, Höhler T, Galle PR, Büchler MW. 2005. Colorectal cancer. The Lancet, 365(9454):153–165.

Xu H, Rice BW. 2009. In-vivo fluorescence imaging with a multivariate curve resolution spectral unmixing technique. Journal of Biomedical Optics, 14(6):064011.

Yao Z, Zhang BS, Prescher JA. 2018. Advances in bioluminescence imaging: New probes from old recipes. Current opinion in chemical biology, 45:148–156.

Youssof AME, Alanazi FK, Salem-Bekhit MM, Shakeel F, Haq N. 2019. Bacterial Ghosts Carrying 5-Fluorouracil: A Novel Biological Carrier for Targeting Colorectal Cancer. AAPS PharmSciTech, 20(2):48.

Zelmer A, Ward TH. 2013. Noninvasive fluorescence imaging of small animals. Journal of Microscopy, 252(1):8–15.

Zhang C, Zhao Z, Li J, Song K-G, Hao K, Wang J, Wang G-X, Zhu B. 2019. Bacterial ghost as delivery vehicles loaded with DNA vaccine induce significant and specific immune responses in common carp against spring viremia of carp virus. Aquaculture, 504:361–368.

Zhang S. 2016. Ex Vivo Imaging, Biodistribution, and Histological Study in Addition to In Vivo Imaging. In: Bai M, Editor In Vivo Fluorescence Imaging: Methods and Protocols. New York, NY: Springer; 183–191

Zink FE. 1997. X-ray tubes. Radiographics: A Review Publication of the Radiological Society of North America, Inc, 17(5):1259–1268.

List of figures and tables